

Syracuse University

**SURFACE**

---

Theses - ALL

---

January 2017

## **A material characterization of two-solution bone cement containing ethylene glycol-dimethacrylate as a crosslinker**

Michael John Wiegand  
*Syracuse University*

Follow this and additional works at: <https://surface.syr.edu/thesis>



Part of the [Engineering Commons](#)

---

### **Recommended Citation**

Wiegand, Michael John, "A material characterization of two-solution bone cement containing ethylene glycol-dimethacrylate as a crosslinker" (2017). *Theses - ALL*. 139.  
<https://surface.syr.edu/thesis/139>

This is brought to you for free and open access by SURFACE. It has been accepted for inclusion in Theses - ALL by an authorized administrator of SURFACE. For more information, please contact [surface@syr.edu](mailto:surface@syr.edu).

## **Abstract**

Bone cements are primarily used for fixation of implants as well as dampening of mechanical loads between the implant and neighboring bone. Two-solution bone cements offer a variety of advantages over commercial powder-liquid compositions due to a reduction in porosity, which in turn leads to improved mechanical properties. The effectiveness of the material is limited by its mechanical properties due to a large mismatch in moduli and strength between the cement, bone, and implant. Two-solution bone cements modified with ethylene glycol-dimethacrylate (EG-DMA) as a crosslinker have been developed as an attempt to further improve the mechanical and thermal properties of the material. The crosslinker replaces a volumetric portion of the methyl methacrylate (MMA) monomer and the resulting mechanical, thermal and viscous properties were compared to a formulation free of EG-DMA.

The result of this study shows that EG-DMA can increase the mechanical properties and fractional monomer conversion without significantly ( $p < 0.05$ ) affecting the thermal characteristics, including maximum polymerization temperature and setting time. The maximum flexural strength and bending modulus increase with increasing EG-DMA concentrations up to 10 vol% EG-DMA, and then decrease following a second order polynomial fit. The critical stress intensity factor increases up to 5 vol% and then decreases with increasing EG-DMA content, and the yield strength increases up to 15 vol% EG-DMA. These results indicate that up to a certain concentration, EG-DMA vol% has more of an effect on a specific mechanical property than decreasing the MMA concentration.

All EG-DMA compositions had a higher viscosity than the control at all measurable shear rates due to a higher polymer to MMA ratio. These formulations demonstrated an increase in ductility and the fractured samples displayed different surface morphologies than the control samples.

Sample sets containing EG-DMA did not fracture at the upper strain limit (10%) during flexural tests, except 10 and 15 vol% EG-DMA. The fractured EG-DMA samples exhibited evidence of large amounts of plastic strain before failure, indicated by micro-troughs and ridge formation. Samples containing 20 vol% EG-DMA had the highest fractional monomer conversion and lowest residual monomer concentration. This was attributed to the high reactivity of EG-DMA molecules in the presence of an initiator.

These formulations provide insight into the effect of substituting a crosslinker for MMA monomer in a two-solution injection system and layout the ideal concentrations of EG-DMA for superior mechanical or fractional monomer conversion properties.

A MATERIAL CHARACTERIZATION OF TWO-SOLUTION BONE CEMENT  
CONTAINING ETHYLENE GLYCOL-DIMETHACRYLATE AS A CROSSLINKER

by

Michael Wiegand

B.S., Clarkson University, 2013

Dissertation

Submitted in partial fulfillment of the requirements for the degree of  
Master of Science in *Bioengineering*.

Syracuse University

May 2017

Copyright © Michael Wiegand 2017  
All Rights Reserved

## **Acknowledgements**

The work presented in this thesis would not have been made possible without the support and effort from several people. I would like to thank first and foremost my thesis advisor, Dr. Julie Hasenwinkel. She has guided me through every step of the way during my time at Syracuse University, and her patience and understanding made this process very simple and straightforward. Thank you for giving me all the tools I needed to be successful, and allowing me to join your research group and training me on all the equipment and procedures that you have mastered over the years. Also, thank you for putting up with me being injured about half the time that I came to your office.

I am thankful for the good relations I have developed with my committee members, Dr. Michelle Blum and Dr. Pranav Soman, during my time in the SBI. I would also like to thank my other committee member, Dr. Jeremy Gilbert, for providing me with additional and future research opportunities and guidance. I look forward to continuing my work under his direction. I would like to acknowledge all professors and staff of the Syracuse Biomaterials Institute and the Department of Biomedical and Chemical Engineering. Thank you to Lynore de la Rosa and Karen Low for helping me around the SBI with whatever needs I had. I thank Syracuse University for all the assistantships and fellowships that have supported me financially.

I am thankful for all my friends that have made my time at Syracuse as enjoyable as possible. Kennedy Faraci and Brittany Reed both contributed to this work and were very eager to help as my research mentees. I would also like to thank my fellow researchers and roommates Allen Osaheni and Srihari Prasad. Living with two other graduate students made life easier when I left campus as I didn't really have to justify my moods or strange work hours, it was just understood. Thank you also to my former mentor at Bristol-Myers Squibb, Dr. Terrance Carone, for

encouraging me to pursue my degree at Syracuse University and to work with Dr. Hasenwinkel. Thank you for continuing to offer your guidance and instruction.

Lastly, I would like to thank my amazing family. My parents, Kevin and Caroline, and my sister Allison have been there for me every step of the way. I am extremely grateful for their unwavering support and love during this process, as well as trying their best to remain interested when I talk about chemicals and cement. I would also like to thank my grandfather Richard Oden for providing me inspiration and motivation to go into the field of biomedical engineering. I witnessed him receive two total knee replacements and from that point on, I knew what field I wanted to go into.

Thank you.

## Table of Contents

Abstract.....	i
Acknowledgements.....	v
Section 1: Introduction.....	1
Section 2: Specific Aims.....	5
Section 3: Goals and Hypotheses.....	5
Section 4: Materials and Methods.....	7
4.1: Cements preparation.....	7
4.2: Exothermal properties of cements.....	9
4.3: Viscosity measurement.....	10
4.4: Fracture toughness.....	11
4.5: Flexural properties.....	12
4.6: DSC technique.....	13
4.7: Calculation of monomer conversion parameters.....	15
4.8: Optical microscopy and SEM observations.....	18
4.9: Statistical analysis.....	18
Section 5: Results.....	18
5.1: Exothermal characteristics of modified cements containing EG-DMA.....	18
5.2: Fracture toughness analysis.....	20
5.3 Flexural properties.....	21
5.4: Conversion, exothermic heat, concentration of residual monomer and glass-transition temperature.....	23
5.5: Viscosity analysis.....	26
5.6: Scanning electron microscopy and optical imaging.....	30
Section 6: Discussion .....	32
Section 7: Conclusion.....	37
Section 8: Future Work.....	38
Appendices.....	40
References.....	45
Vita.....	48



## 1. Introduction

Poly(methyl methacrylate) (PMMA) based bone cements have been used primarily in implant fixation and joint replacements since their development in 1958 and commercialization in the 1960s (1). The cements fill the space between the bone and device, and harden *in vivo* through a free radical polymerization process resulting in a strong acrylic material. The primary functions of bone cements are to stabilize implants and provide cushioning to the bone by transferring of mechanical loads (2). The liquid component of bone cements is methyl methacrylate (MMA), an ester of methacrylic acid (1, 2). The liquid component also contains *N-N*-dimethyl-*p*-toluidine (DMPT), a tertiary aromatic amine and hydroquinone (HQ), an inhibitor. The powder component consists principally of pre-polymerized PMMA beads or PMMA based polymers and benzoyl peroxide (BPO), an initiator (2). When the BPO and DMPT molecules are mixed, a redox reaction occurs and produces free radicals that trigger the cascade of MMA monomer polymerization (3). The monomer polymerizes around the PMMA beads, creating a 'homogeneous' network of PMMA beads surrounded by newly polymerized PMMA. While PMMA based bone cements are considered the gold standard in implant fixation (1,2), there exists several drawbacks that limit the effectiveness of the material.

Acrylic bone cements undergo highly exothermic reactions due to carbon-carbon double bonds being broken during polymerization. Temperatures at the bone-cement interface can reach up to 10° above physiological temperature (37°C) (4, 5). Thermal necrosis can occur in excess of 47°C and protein denaturation can occur at 56°C (4). Chemical necrosis is also a factor with bone cement due to residual MMA monomer present at the surface. Monomer can also leach out of the cement after a prolonged amount of time (6). DMPT has also been shown to have cytotoxic effects as well (5). Residual monomer can also have adverse effects on the mechanical properties

of the material. The concentration of residual monomer changes over time due to a slow-continued polymerization after the initial reaction, thus slowly changing the overall molecular and mechanical properties of the material (7).

The clinical success of bone cements is limited by poor mechanical properties, specifically weakness in tension, shearing and fatigue resistance (2, 6). These weaknesses can lead to aseptic loosening of the implant at either the implant-cement or cement-bone interface. Large mismatches in moduli between the cement and surrounding bone can cause crack propagation throughout the material and debonding of the material at the cement-bone interface (8). Cement particles as a result of fracture can induce osteolysis at the bone-cement interface, further loosening the implant and ultimately resulting in failure (6). Bone cement failure can also occur from porosity. Porosity can transpire from five different sources: (I) air within the powder components, (II) air trapped within the liquid-powder mixture during initial wetting, (III) bubble accumulation during stirring of the bone cement system, (IV) air trapped after cement delivery within the mixture or along the implant/bone interfaces and (V) monomer volatilization due to heat generation during the initial curing (9). Volumetric shrinkage is another concern during the polymerization of bone cement. When the low density monomer is converted to a polymer of higher density, shrinkage materializes creating porosity (3). The use of difunctionalized methacrylates such as triethyleneglycol-dimethacrylate have shown a decrease in shrinkage with an increase in mechanical properties (10, 11).

Hasenwinkel et al. (3) developed a two-solution bone cement (TSBC) that is highly-viscous and injectable for the purpose of joint prostheses fixation while eliminating many of the known setbacks previously described. It was found that concentrations of BPO and DMPT significantly affected polymerization temperatures and setting time as well as flexural properties. A molar

ratio of 1 (BPO:DMPT) optimized the flexural strength and modulus of the cement (3). The mixing process developed also eliminated porosity traditionally introduced in the preparation of the material. The cement is prepared by dissolving the powder components in the liquid monomer, mixing for 18 hours and then letting it sit upright in cold storage for 2 days (3). Letting the cement sit in cold storage for 2 days allows any bubbles generated to rise to the top of the material (3). Additionally, the two-solution bone cement has a shelf life up to 12 months due to the stability of the initiator (BPO) in cold storage (4°C) (12). The TSBC was further modified by the addition of crosslinked-PMMA microspheres and nanospheres. The crosslinked PMMA beads do not dissolve in the monomer resulting in a higher polymer to monomer ratio. The use of the crosslinked particles reduced the maximum polymerization temperature due to the decreased concentration of monomer. This modification resulted in higher degrees of shear thinning, with the nanospheres having more of an effect on the pseudoplasticity of the cement than the microspheres. These formulations had similar mechanical properties to the standard TSBC (3), making it a suitable candidate for vertebroplasty applications (13, 14). Additionally, grafting PMMA brushes on the surface of the crosslinked PMMA nanospheres resulted in a larger degree of swelling by the PMMA particles while maintaining a suitable viscosity. These alterations were primarily aimed at three areas of improvement: (I) improving the bonding between the PMMA beads and the polymerized cement matrix, (II) increasing the resulting molecular weight of the cement and (III) improving the mechanical properties (13, 14).

Ethylene glycol-dimethacrylate (EG-DMA) is a biodegradable difunctional crosslinker and an appealing material for bone cement additives because of its ability to be used as a crosslinker between adjacent PMMA chains (15). Alves et al. and Sasaki et al. (16, 17) both found that crosslinking PMMA chains with EG-DMA molecules increases the material's glass-transition

temperature and yield stress due to a reduction in molecular mobility between PMMA chains.

Min et al. reported that when PMMA chains lightly crosslinked with 1 mol% EG-DMA undergo shear loading, the carbon backbone degree of alignment increases (15). The backbone aligns with the direction of external loading, thus decreasing the force per area and deformation exhibited on the main carbon bonds. This resulted in an increase in ductility in the lightly crosslinked PMMA chains (15).

EG-DMA molecules contain twice as many double bonds as MMA molecules, and the reactivity and heat generated during the breaking of the first double bond has been estimated to be indistinguishable to that of MMA (18). The addition of EG-DMA to a free radical polymerization system can also lead to the formation of other species in addition to linear crosslinked chains. EG-DMA molecules can remain unreacted, react once (one double bond remains unreacted) or form cyclic species (18). Yang et al. (19) studied the effects of adding varying concentrations of EG-DMA and hydroxyethyl methacrylate (HEMA) to PMMA based bone cements. HEMA is a monomer with one carbon-carbon double bond. HEMA and EG-DMA decreased the Young's modulus and polymerization time while increasing the tensile, bending and compressive strengths, as well as the polymerization temperature. Vallo et al. (20) prepared self-curing bone cements with crosslinked PMMA beads using two different crosslinkers with different chain lengths: triethyleneglycol-dimethacrylate (TEGDMA) and poly(ethylene glycol)-dimethacrylate (PEG-DMA) (21). The cement compositions containing the crosslinked PMMA beads displayed a higher flexural modulus with a decrease in yield strength. SEM images revealed a prominent bonding effect between the crosslinked beads and the polymerized PMMA matrix (20). Zuk et al. (22) studied the effect of polymer impregnated concrete (PIC) using methyl methacrylate (MMA) and ethylene glycol-dimethacrylate (EG-DMA) as the monomer

constituents. Their work showed that PIC with EG-DMA increased the compressive strength and adhesive properties, as well as the polymerization yield due to the high reactivity of EG-DMA monomer in the presence of an initiator (BPO) (22).

## **2. Specific Aims**

- I. Modify two-solution bone cement (TSBC) with varying levels of ethylene glycol-dimethacrylate (EG-DMA) crosslinker
- II. Assess mechanical properties of polymerized TSBC modified with EG-DMA using three-point bend tests and fracture toughness tests
- III. Characterize real-time thermal properties of cement compositions during free radical polymerization
- IV. Measure viscosity profiles for compositions
- V. Analyze fracture surfaces and morphology of fractured mechanical samples

## **3. Goals and Hypotheses**

We hypothesize that synthesis of an injectable two-solution bone cement (TSBC) modified with ethylene glycol-dimethacrylate (EG-DMA) will be advantageous over other materials used for the same application because it will have increased strength and similar thermal properties. The strength will be increased due to localized crosslinking between adjacent PMMA chains. We predict that the thermal properties will be similar due to compositions having similar amounts of carbon-carbon double bonds available for polymerization. The characterization and supplemental research associated with this material will focus on measuring the mechanical properties, recording the real-time polymerization process and the resulting properties such as residual

monomer content and fracture morphology. All compositions of modified TSBC with EG-DMA will be tested against a control composition containing 0 vol% EG-DMA.

We hypothesize that the viscosity will increase across all modified compositions. PMMA is not soluble in EG-DMA and by increasing the polymer to MMA ratio, more polymer is being dissolved in less MMA and thus creating a more dense and viscous slurry. EG-DMA is also more viscous at ambient temperature than MMA.

We hypothesize that the addition of the crosslinker will increase mechanical properties with increasing EG-DMA concentrations. Increasing the crosslink density of a polymer matrix increases the modulus (15). The crosslinker will increase the material's resistance to deformation along the PMMA carbon backbone (15), and this will increase the strain-to-failure of the modified cements.

We anticipate the thermal properties to be consistent and like that of the control. The double bond ratio (DB), ratio of double bonds in the modified sample to the control sample, increases by 3% when increasing the EG-DMA concentration up to 25 vol%. The moles of monomer initially present decreases up to 11% (25 vol%) with increasing EG-DMA concentrations (Table 4.1.1). While there will be more double bonds available to break and release heat, there will be less total moles available to react with one another. We predict that these relationships will have counteracting effects on the system and not significantly change the thermal properties. EG-DMA molecules are more reactive than MMA molecules (22) and therefore we anticipate that the total fraction of monomer molecules converted will increase with increasing EG-DMA concentrations. We also hypothesize that the glass-transition temperature ( $T_G$ ) will increase in the EG-DMA formulations due to an increase in crosslink density. Increasing the crosslink density

will reduce the chain mobility in the cured sample, which is directly related to the glass-transition temperature (15).

Finally, we hypothesize that the fracture surface morphology will be different than the control TSBC due to the increased crosslinking. The crosslinking will alter the fracture mechanism due to the increased strain-to-failure. We predict that because the material will be subject to increased strain, the surfaces will display troughs and micro-sized craters along the fractured edge (23).

## **4. Materials and Methods**

### *4.1 Cements preparation*

PMMA resin (Monomer Polymer) (80,000 g/mol), MMA (Aldrich), EG-DMA (Aldrich) benzoyl peroxide (BPO) (Aldrich) and *N,N*-dimethyl-*p*-toluidine (DMPT) (Aldrich) were used as received in all compositions. The preparation of all cements followed the technique developed by Hasenwinkel et al. (3). Previously described two-solution bone cements (TSBCs) containing a polymer to monomer (g:mL) ratio (P:M) of 0.9:1 developed by Hasenwinkel et al. (3) served as the control for all experiments performed. Compositions containing EG-DMA had a fixed polymer to liquid (g:mL) ratio (P:L) of 0.9:1 with varying MMA to EG-DMA ratios (See Table 4.1.1). The molar ratio of EG-DMA to MMA is also given in Table 4.1.1. The PMMA resin was massed and set aside to be the polymer component for all compositions. The total MMA and EG-DMA volume was split equally between two beakers, in which one contained 1.25 g of BPO and the other contained 0.7 mL of DMPT. The BPO to DMPT (mol:mol) ratio was fixed for all compositions at 1, and the total liquid volume was set at 100 mL for all compositions. The MMA solutions were mixed thoroughly to ensure complete dissolution of the BPO powder and DMPT liquid. The two solutions were then transferred to two polypropylene cartridges followed by the

addition of the polymer resin. The cartridges were sealed, shaken by hand for 5 minutes and transferred to a rotating drum mixer for 18 hours at room temperature.

**Table 4.1.1: Sample compositions by volume percentage, volume ratio, moles, molar ratio, and double bond (DB) ratio between the control and modified compositions**

	Control	2.5EGDMA	5EGDMA	10EGDMA	15EGDMA	20EGDMA	25EGDMA
EG-DMA vol%	0	2.5	5	10	15	20	25
MMA vol%	100	97.5	95	90	85	80	75
EG-DMA: MMA (mL:mL)	0	0.03	0.05	0.11	0.18	0.25	0.33
EG-DMA moles	0	0.0132	0.0265	0.0530	0.0795	0.1060	0.1325
MMA moles	0.9388	0.9153	0.8919	0.8449	0.7980	0.7510	0.7041
Total moles	0.9388	0.9286	0.9184	0.8979	0.8775	0.8571	0.8367
EG-DMA mol%	0	1.42	2.88	5.90	9.06	12.4	15.8
DB Ratio	1.000	1.003	1.006	1.012	1.019	1.025	1.032

After mixing, cartridges were removed and stored upright at 4°C for 48 hours before use.

Volumetric ratios (mL:mL) of MMA to EG-DMA ranged from 100:0 to 75:25. Compositions used for viscosity tests were prepared the same with the exception of the BPO and DMPT components. This was to prevent the cement from polymerizing in the viscometer testing chamber. Viscosity samples were also prepared in smaller cartridges using the same proportions as above. This was due to the small size of the testing chamber. Cartridges were stored upright to allow any bubbles generated in the mixing process to rise to the top, thus eliminating a source of porosity during the curing process.



#### 4.2 Exothermal properties of cements

The maximum polymerization temperatures and setting times of the modified TSBCs were measured using the ASTM standard F451 (25) and an in-house thermocouple sensing unit. The thermocouple wire was soldered to create one point of contact, and the tip of the soldered wire was placed so it was directly in the center of the mold, both vertically and concentrically. All measurements were compared to the control TSBC. The maximum polymerization temperature is defined as the peak temperature during the initial curing after injection into the mold. Setting time (Figure 4.2.1) corresponds to the time at which the average temperature between ambient

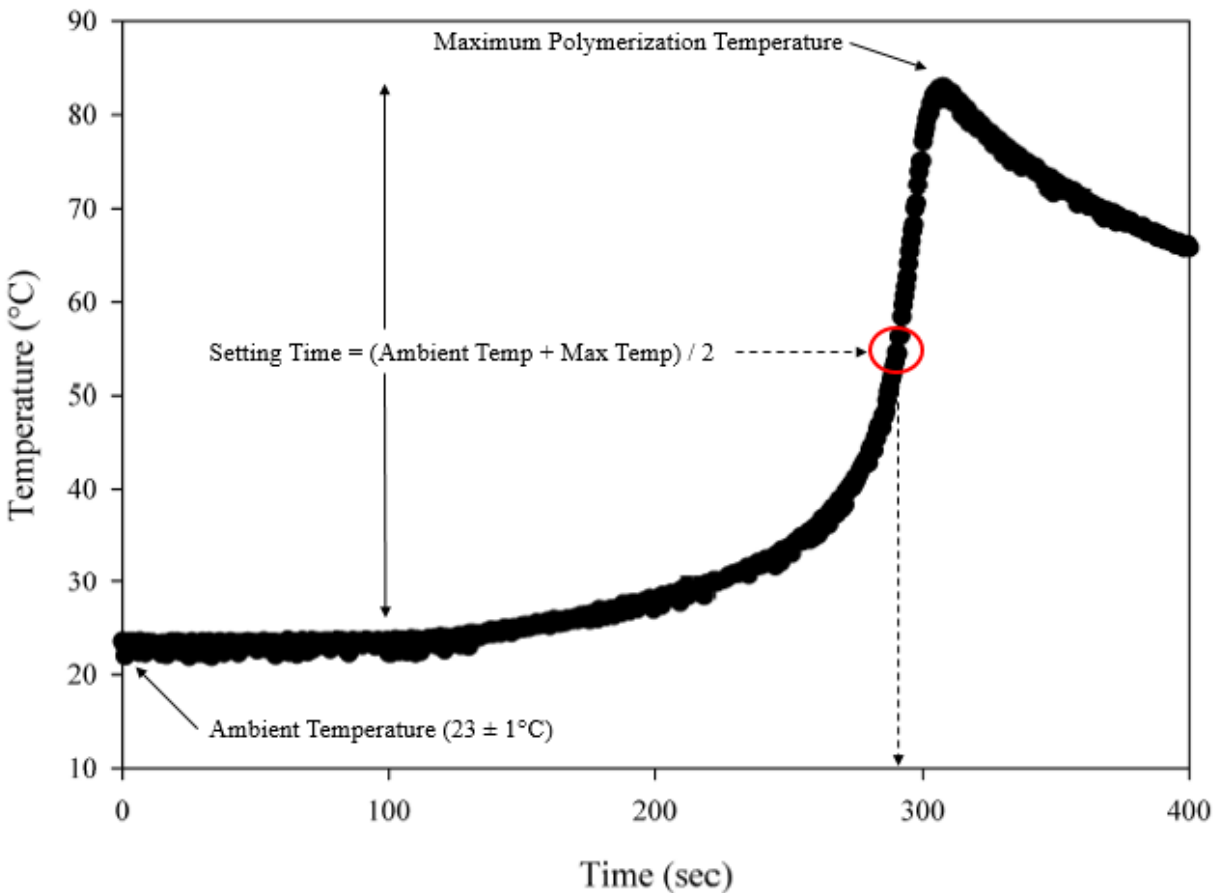


Figure 4.2.1: Exothermal experimental output. Experiment begins when the cement first mixes in the nozzle and ends after a vertex temperature has been recorded. The setting time is defined as the time corresponding with half of the ambient temperature added to the maximum polymerization temperature. The above figure is for the control TSBC.

( $23\pm 1^\circ\text{C}$ ) and peak temperature is reached (25). Each composition was tested in triplicate ( $n=3$ ) and reported as an average with data points taken at every 0.5 seconds. Tests began when the cement first started mixing in the nozzle. The pneumatic gun forced the material into the mold and the mold was screwed closed after it was filled completely. Tests ceased after the maximum temperature was reached and the material began to cool. The polyethylene molds were cleaned and cooled to ambient temperature after each trial. Average maximum polymerization temperatures and setting times were reported and standard deviations were calculated.

#### *4.3 Viscosity measurement*

The viscosities of the modified TSBCs and control TSBC were measured using a digital rotational viscometer (Brookfield Viscometer DV-E) with a coaxial spindle (SC4-14). The viscometer was calibrated before measurements were taken using 60,000 cP (60 Pa·s) silicone oil calibration standards (Brookfield Engineering Laboratories Inc.) to ensure accurate readings within +/- 1% of the machine's sensitivity. Viscosity tests were performed at ambient temperature with the sample cartridges sitting out for a minimum of 3 hours prior to testing. Materials were injected into the sample chamber until the chamber was 3/4 full. The chamber then slid up into the viscometer with the spindle attached, and material was injected around the spindle until the chamber was full. The top of the chamber was covered with aluminum foil to prevent volatilization of the material. Rheological measurements were performed at increasing rotational speeds (0.3 to 100 RPM) and recorded at all readings between the lower and upper torque limits ( $10\% \leq \text{Torque} \leq 100\%$ ). Measurements were taken every 30 seconds for 5 minutes at each RPM, and each composition was tested using the same spindle (SC4-14). Shear rate is proportional to speed for a given spindle and the RPM was multiplied by a correction factor based on spindle+chamber geometry used ( $\times 0.4$  for SC4-14). Compositions were tested three

times at increasing shear rates and average viscosities and standard deviations of all trials were reported. The spindle and viscometer chamber were cleaned in between each trial to ensure all previous material had been removed.

#### 4.4 Fracture toughness

Fracture toughness tests were performed per ASTM standard E399-83 (26) for plain-strain mode I failure of at least four bone cement samples for each composition. Materials were injected into rectangular polyethylene molds and allowed 30 minutes to polymerize. After the initial polymerization, samples were stored in the lab at room temperature overnight and wet polished the next day using 240, 320, 400 and 600  $\mu\text{m}$  grit sandpaper. Finished samples were polished on all sides in a uniform direction. This was to ensure consistent flat surfaces. The polyethylene mold had an average width of 11.5 mm and average thickness of 3.25 mm, and polishing resulted in samples having slightly smaller measurements. After polishing, a notch was made in each sample using a slow speed diamond cut-off wheel (Buehler, Isomet Low Speed Saw) and a sharp crack tip was made using a razor blade and a hammer. The length of each crack ( $a$ ) (including the sharp crack tip) was between  $0.45W \leq a \leq 0.55W$  where  $W$  is the sample width. Cracks were made at the midway point of the sample length. The samples were tested at room temperature on a Sintech MTS system (model 2GT) using a crosshead speed of 2.54 mm/min. The span length between the machine fixtures measured 40 mm with the crosshead beam placed at the center above the sample. Mode I plane strain fracture toughness was calculated using Equation 4.4.1:

$$K_{IC} = \frac{PL}{bW^{3/2}} * \frac{3\left(\frac{a}{W}\right)^{1/2} \left[1.99 - \left(\frac{a}{W}\right) \left(1 - \frac{a}{W}\right) * \left(2.15 - 3.93\frac{a}{W} + 2.7\frac{a^2}{W^2}\right)\right]}{2\left(1 + 2\frac{a}{W}\right) \left(1 - \frac{a}{W}\right)^{3/2}} \quad (4.4.1)$$

where  $K_{IC}$  is the critical stress intensity factor ( $\text{MPa}\sqrt{\text{m}}$ ),  $P$  is the maximum load (N),  $L$  is the span length (mm),  $b$  is the sample thickness (mm),  $W$  is the sample width (mm) and  $a$  is the crack length

(mm). The critical stress intensity factor or fracture toughness was reported as an average for each sample set with calculated standard deviations.

#### 4.5 Flexural properties

Three point flexural tests were performed using ASTM D790-86 standards (27) for five samples of each composition. The samples were polymerized and wet-polished using the same procedures as the fracture toughness tests (Section 4.4). Samples were tested using a Sintech MTS system (model 2GT) with a crosshead speed of 2.54 mm/min and a span support length of 40 mm. Equations 4.5.1-4.5.3 were used to calculate maximum stress ( $\sigma$ ), flexural modulus ( $E_b$ ), and maximum strain ( $\epsilon$ ).

$$\sigma = \frac{3PL}{2bd^2} \quad (4.5.1)$$

$$E_b = \frac{L^3M}{4bd^3} \quad (4.5.2)$$

$$\epsilon = \frac{6Dd}{L^2} \quad (4.5.3)$$

where  $P$  is the maximum load (N),  $L$  is the span support length (mm),  $M$  is the slope of the load/crosshead displacement curve (N/mm),  $b$  is the sample width (mm),  $d$  is the sample thickness (mm) and  $D$  is the maximum deflection measured by the crosshead beam (mm). Yield stress was calculated by determining the equation of the elastic deformation section of the stress-strain curve, and then applying an offset of 0.2% and determining where the offset linear equation (Equation 4.5.4) intercepted the raw data.

$$\sigma_{Yield} = (E_s x + 0.002) + y_o \quad (4.5.4)$$

where  $E_s$  is the slope of the linear region of the  $E_b$  data (~0 and 1.5% strain),  $x$  is the sample strain data (Equation 4.5.3) and  $y_o$  is the y-intercept. The slope and y-intercepts were calculated using a linear regression model in Excel (Microsoft). The yield stress is found when Equation 4.5.4 subtracted from Equation 4.5.1 is equal to zero. Maximum flexural stress, bending (flexural)

modulus, yield stress and strain-to-failure were reported as averages for sample sets and standard deviations were calculated.

#### *4.6 DSC technique*

All differential scanning calorimetry experiments were performed under isothermal conditions at 50°C. Following isothermal testing, the sample chamber was ramped from 50°C to 150°C at a heating rate of 10°C/min. All trials were performed using a TA Q200 differential scanning calorimeter (TA). The DSC generates the data in W/g, therefore accurate readings require the mass of the sample beforehand. The heating rate (10°C/min) was chosen based off previous observations in the literature and in the Hasenwinkel lab (14). At lower heating rates (< 5°C/min), there exists limitations in capturing the complete methyl methacrylate conversion of the free radical polymerization (28). Samples were taken out of cold storage for 3 hours prior to testing and allowed to heat up to room temperature. It was necessary to perform the experimental set-up in as little time as possible (< 2 minutes) to ensure the machine captured the entire curing exotherm during the onset of polymerization. Hermetic pans and lids were massed before injection and recorded. Hermetic pans were chosen because the sample's material properties changed throughout the course of the experiment due to the volatile properties of the methyl methacrylate monomer (29). Samples approximately 30-40 mg were injected into the pans through a static mixing nozzle and the pans were hermetically sealed with the aluminum lid immediately. Samples were remassed and the mass of the sample was calculated by subtracting the empty pan+lid mass from the new injected mass. The samples were then placed in the DSC chamber alongside an empty reference pan+lid and the experimental protocol began. Samples were held isothermally at 50°C for one hour followed by one heating cycle, one cooling cycle and a second heating cycle. All non-isothermal cycles were heated and cooled at a rate of 10°C/min with heating cycles

increasing from 50°C to 150°C and the cooling cycle decreasing from 150°C to 50°C. There was also an isothermal hold at the end of each non-isothermal cycle for 2 minutes before the next cycle began. This was to allow the material to stabilize at the upper and lower temperatures before the next cycle began. Markers were placed at the end of all isothermal and non-isothermal cycles for analysis purposes. Table 4.6.1 describes the method file used for all DSC experiments.

**Table 4.6.1: Method file for isothermal and non-isothermal DSC**

Method File
Jump to 50.00 °C
Isothermal for 60.00 min
Mark end of cycle 1
Ramp 10.00 °C/min to 150.00 °C
Isothermal for 2.00 min
Mark end of cycle 2
Ramp 10.00 °C/min to 50.00 °C
Isothermal for 2.00 min
Mark end of cycle 3
Ramp 10.00 °C/min to 150.00 °C
Isothermal for 2.00 min
Mark end of cycle 4

The isothermal steps are marked in blue and the non-isothermal steps of the method file are marked in red in Table 4.6.1. The temperature ramps were performed for two fundamental reasons: (I) to ‘drive’ the reaction to completion by converting residual monomer that is either vitrified or lacks nearby free radicals and (II) to observe the glass-transition temperature in the final cured sample (29). The first non-isothermal scan will reveal a small peak (Figure A.1) that represents the residual monomer. This exothermic peak is not present in the second non-isothermal scan and thus the

inflection point, signifying the onset of molecular motion (glass-transition temperature) (24), can be measured (Figure A.2). Setting time could not be measured due to the nature of this experiment but the heat of reaction, degree of conversion, residual monomer concentration and glass-transition temperature were all measured or calculated. Samples were tested in triplicate. Averages were reported and standard deviations were calculated.

#### *4.7 Calculation of monomer conversion parameters*

The heat of reaction, also referred to as the change in enthalpy, can represent both exothermic and endothermic processes. Exothermic processes are a release of heat while endothermic processes take in or absorb heat (24). The power recorded (W/g) during the first hour of the isothermal DSC scan can be integrated and transformed into exothermal heat per mole (kJ/mol), and compared to known heats of reaction for methyl methacrylate (56.9 kJ/mol MMA) (21, 30). The DSC uses the reference pan to accurately match the temperature of the reference pan to that of the sample pan. As the temperature of the sample pan increases during curing, the machine adds heat to the reference pan to match the sample pan heat, thus generating a heat flow. When the sample pan no longer produces heat after the initial polymerization peak, the free radical reaction is over or fell below the detection capability of the machine. After each trial was completed, each curve was individually analyzed by integrating the power versus time for a period up to one hour. This integral represents the total heat given off during the initial polymerization of the bone cement and each composition was tested in triplicated. Compositions were prepared using the same material proportions as Section 4.1, but in smaller cartridges and smaller static mixing nozzles due to the size of the hermetic pans. The first step in analyzing the DSC data is normalization of the exothermal curve using Equation 4.7.1.

$$P(t) = [AP(t) - AP(endtime)] \quad (4.7.1)$$

where  $P$  is the normalized power (W/g),  $AP$  is the power (W/g) and  $t$  is the time domain. The power value at the end of the isothermal process represents the baseline and this value is subtracted from all values for individualized baselines (Figure A.1). To estimate the total heat generated during polymerization, a power-time function was applied to all integrated data. The algorithm in Equation 4.7.2 was used to perform this function.

$$H_{cumulative} = \sum_{n=0}^{n-1} \left\{ \frac{P_{n+1} + P_n}{2} \times (t_{n+1} - t_n) \right\} \quad (4.7.2)$$

where  $H_{cumulative}$  is the cumulative heat of polymerization (J/g),  $P$  is the normalized power (W/g) and  $t$  is the time domain (s). The total heat ( $H_{curing}$ ) (kJ/mol) generated is calculated using Equation 4.7.3 using the correction factor in Equation 4.7.2.

$$H_{curing} = \frac{MW_{MMA} * Mf_{MMA} + MW_{EG-DMA} * Mf_{EG-DMA}}{f} \sum_{n=0}^{n-1} \left\{ \frac{P_{n+1} + P_n}{2} \times (t_{n+1} - t_n) \right\} \quad (4.7.3)$$

where  $MW_{MMA}$  and  $MW_{EG-DMA}$  are the molecular weights (g/mol) of MMA and EG-DMA monomer, respectively,  $Mf_{MMA}$  and  $Mf_{EG-DMA}$  are the mass fractions for MMA and EG-DMA of the total liquid monomer mass used and  $f$  is the mass fraction of MMA + EG-DMA in the sample. Multiplying the molecular weights by the corresponding mass fraction used for each monomer created a theoretical weight average molecular weight for the sample tested (24). A correction factor was incorporated into the calculations due to the changing amount of double bonds present between EG-DMA concentrations. This was calculated using Equation 4.7.4.

$$DB_f = \frac{DB_n}{DB_0} \quad (4.7.4)$$

where  $DB_f$  is the double bond correction factor,  $DB_0$  is the amount of double bonds present in the TSBC control assuming 100 mL of MMA monomer, and  $DB_n$  is the amount of double bonds present in the composition tested assuming 100 mL of total liquid monomer.  $DB_0$  was determined using Equation 4.7.5.



$$DB_0 = \frac{100 \text{ mL} * \rho_{MMA}}{MW_{MMA}} * \frac{6.022 \times 10^{23} \text{ molecules}}{\text{mole}} * \frac{1 \text{ double bond}}{MMA \text{ molecule}} = 5.6538 \times 10^{22} \text{ double bonds} \quad (4.7.5)$$

where  $\rho_{MMA}$  is the density of the methyl methacrylate (g/mL).  $DB_n$  was calculated using a similar equation, with the inclusion of the EG-DMA component.

$$DB_n = \left[ \frac{V_{MMA} * \rho_{MMA}}{MW_{MMA}} * \frac{6.022 \times 10^{23} \text{ molecules}}{\text{mole}} * \frac{1 \text{ double bond}}{MMA \text{ molecule}} \right] + \left[ \frac{V_{EG-DMA} * \rho_{EG-DMA}}{MW_{EG-DMA}} * \frac{6.022 \times 10^{23} \text{ molecules}}{\text{mole}} * \frac{2 \text{ double bonds}}{EG-DMA \text{ molecule}} \right] \quad (4.7.6)$$

where  $V_{MMA}$  and  $V_{EG-DMA}$  are the respective volumes of MMA and EG-DMA used per 100 mL of monomer for that composition and  $\rho_{EG-DMA}$  is the density of the ethylene glycol-dimethacrylate (g/mL).  $DB_f$  was calculated because as the volumetric ratio of EG-DMA to MMA (mL:mL) increased between compositions, so did the number of theoretical monomer double bonds. As mentioned earlier, the heat generated during the breaking of a one MMA double bond is indistinguishable to that of one EG-DMA double bond breaking (18). This led to the assumption that the total theoretical heat produced is proportional to the amount of double bonds present. The total theoretical heat (100% conversion) produced per mole of MMA is 56.9 kJ (21, 30). The conversion of each sample was found by Equation 4.7.7.

$$X = \frac{H_{curing}}{DB_f * 56.9 \text{ kJ/mol}} \quad (4.7.7)$$

where  $X$  is the fractional monomer conversion. The residual monomer ( $RM$ ) concentration was found using Equation 4.7.8.

$$RM = (1 - X) \times 100\% \quad (4.7.8)$$

The glass-transition temperature was measured using the DSC analysis software (TA Analysis) at the inflection point in the second heating cycle (Figure A.2). All compositions were tested in triplicate (n=3) and the fractional monomer conversion, residual monomer concentration, total heat

generated and glass transition temperatures were reported as an average with corresponding standard deviations.

#### *4.8 Optical microscopy and SEM observations*

Optical imaging and SEM analysis in high magnification were performed for fracture surface analysis. Fracture propagation is usually indicated by a series of semi-circles originating from one central point on the tension surface. Samples were imaged directly in the digital optical microscope (Hirox, KH-8700) using a variety of magnifications before SEM preparation. For the preparation of SEM imaging, samples were dried overnight in a desiccator, gold sputtered (Denton Vacuum, Desk II) for 45 seconds and then transferred to the SEM viewing chamber (JEOL, 5600).

#### *4.9 Statistical analysis*

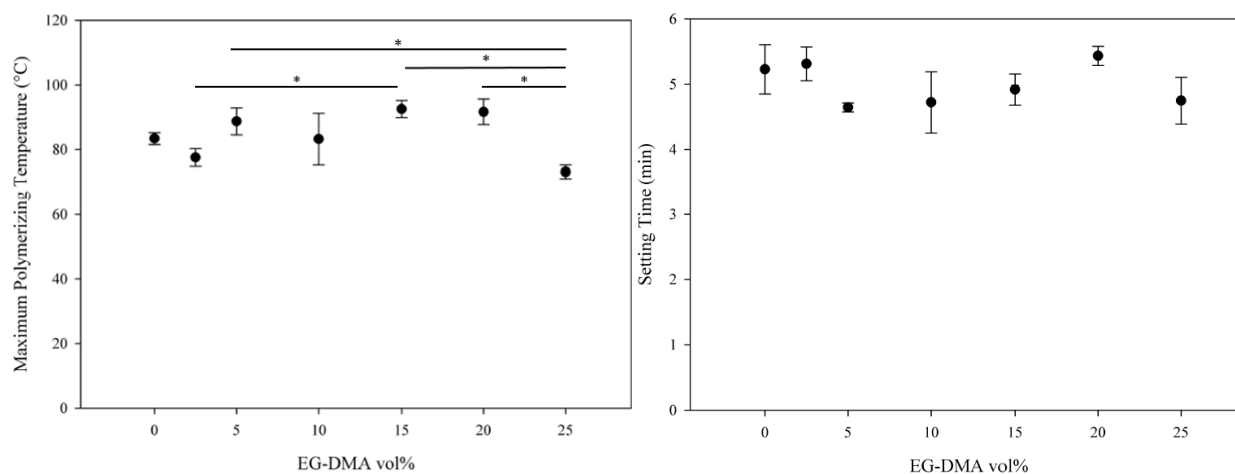
Statistical analysis was performed across all experiments. One-way ANOVA was applied with simple effect and Tukey's *post hoc* comparisons were performed for samples displaying a significant interaction. Significant differences between groups was taken at  $p < 0.05$  and Tukey's comparisons were statistically significant if sample sets didn't share a common grouping. Linear and second-order quadratic fits were applied to data using SigmaPlot 6.0 (Systat) and  $R^2$  values were reported as a measure of fit for data sets that appeared to show a correlation.

## **5. Results**

Appendix C contains data result tables for all experiments as a function of EG-DMA content.

### *5.1 Exothermic characteristics of modified cements containing EG-DMA*

The effect of the substitution of methyl methacrylate monomer for ethylene glycol-dimethacrylate on exothermic behavior of two-solution bone cements was assessed and compared to the standard TSBC previously characterized by Hasenwinkel et al. (3) at a fixed BPO:DMPT molar ratio of 1. Figures 5.1.1 and 5.1.2 show the exothermic characteristics of



Figures 5.1.1 and 5.1.2: Maximum polymerization temperatures and setting times for TSBC and TSBC samples containing EG-DMA. Setting time and maximum polymerization temperatures are plotted as a function of EG-DMA vol%. Sample sets (n=3) that are significantly different ( $p < 0.05$ ) are indicated by an asterisk (\*) and a line that spans between the significantly different sample sets.

TSBCs modified with EG-DMA performed in the standard ASTM mold. There was not a significant change ( $p < 0.05$ ) in maximum polymerization temperature between the control composition (0EGDMA, 83.43°C) and all modified compositions. 25EGDMA's maximum polymerization temperature was significantly lower ( $p < 0.05$ ) than 5EGDMA, 15EGDMA and 20EGDMA's maximum polymerization temperature. 15EGDMA's maximum temperature was significantly higher ( $p < 0.05$ ) than 2.5EGDMA and 25EGDMA. There were no noticeable trends between EG-DMA concentration and maximum polymerization temperature (Figure 5.1.1). The highest temperatures recorded were in excess of 90°C (15EGDMA, 20EGDMA) and the lowest recorded temperatures were below 78°C (2.5EGDMA, 25EGDMA). There was also no significant difference ( $p < 0.05$ ) in any composition's setting time (Figure 5.1.2) when compared with the control cement.

## 5.2 Fracture toughness analysis

Substitution of MMA with EG-DMA

was assessed across all compositions

during fracture toughness analysis

(Figure 5.2.1). Sample sets (n=4) were

tested under the same laboratory

conditions and all samples for a

particular composition set were stored for

the same amount of time before testing. All

samples in one set were tested the same day.

There were no compositions that showed a

significant increase ( $p < 0.05$ ) in fracture

toughness from the control, but compositions containing higher than 5 vol% EG-DMA

(10EGDMA, 15EGDMA, 20EGDMA, 25EGDMA) showed a significant decrease ( $p < 0.05$ ) in

fracture toughness. 10EGDMA had a significantly ( $p < 0.05$ ) lower fracture toughness than samples with a lower EG-DMA concentrations (0EGDMA, 2.5EGDMA, 5EGDMA).

10EGDMA also had a significantly higher fracture toughness ( $p < 0.05$ ) than sample sets containing higher concentrations of EG-DMA (15EGDMA, 20EGDMA, 25EGDMA).

Increasing the EG-DMA concentration from 0 to 5 vol% EG-DMA displayed a rise in fracture

toughness, but not significantly higher than the control TSBC. In compositions higher than 5

vol% EG-DMA, there was a sharp decrease to below half the fracture toughness of the control

(Figure 5.2.1). The maximum critical stress intensity factor ( $K_{IC}$ ) occurred at 5 vol% EG-DMA

(1.6055  $\text{MPa}\sqrt{\text{m}}$ ) and 25 vol% EG-DMA had the lowest critical stress intensity factor at 0.2584

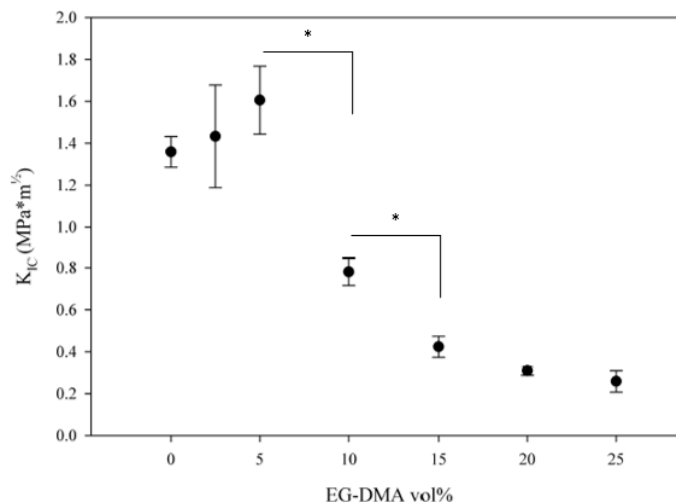


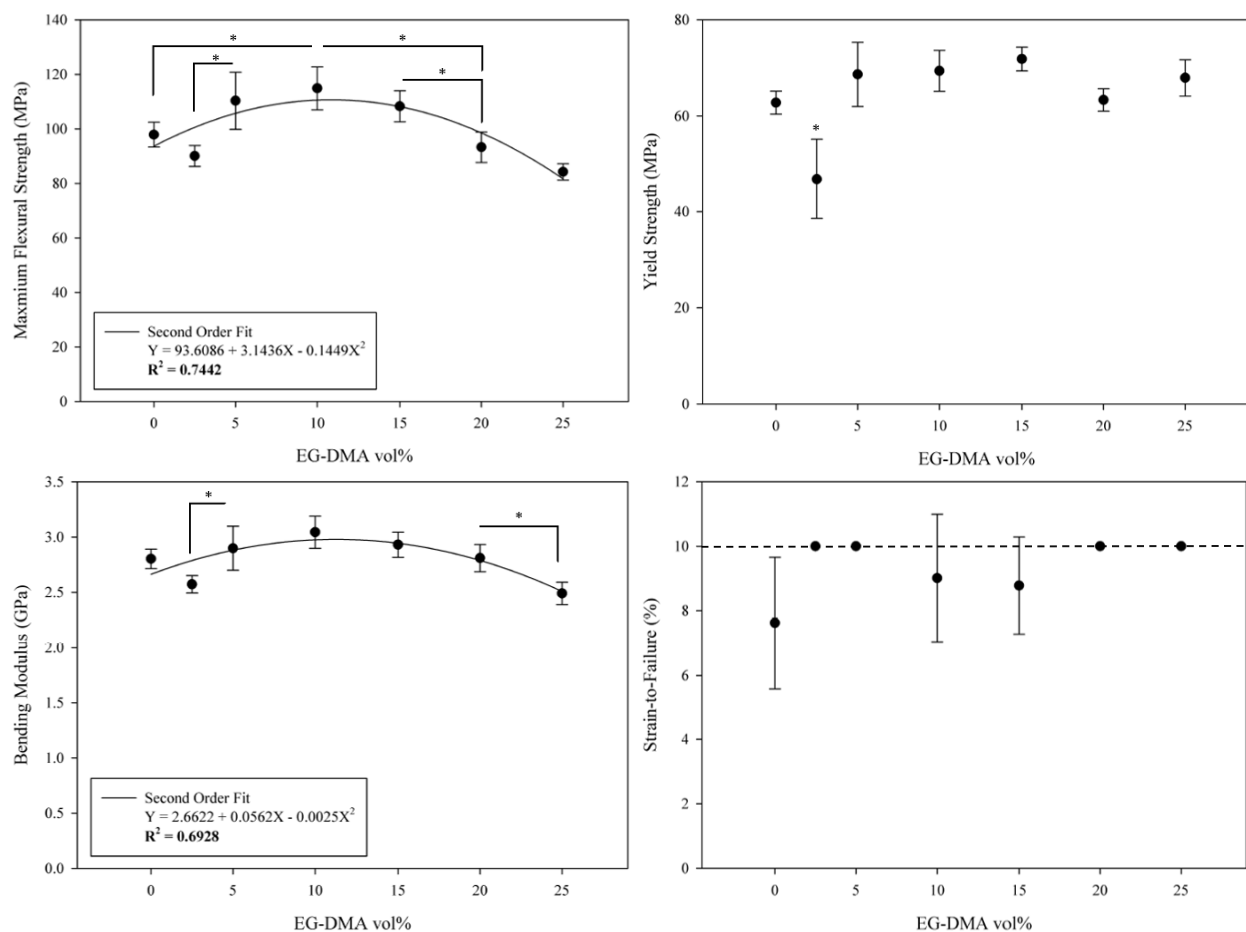
Figure 5.2.1: Critical stress intensity factor ( $K_{IC}$ ) plotted as a function of EG-DMA vol%. Sample sets ( $n \geq 4$ ) that are significantly different ( $p < 0.05$ ) are indicated by an asterisk (\*). Samples containing 0, 2.5 and 5 vol% EG-DMA are not significantly different from each other, and samples containing 15-25 vol% EG-DMA are also not significantly different from each other.

MPa $\sqrt{m}$ . 0EGDMA and 25EGDMA sample sets only contained 4 samples and all other compositions had 5 samples per set.

### *5.3 Flexural properties*

Figures 5.3.1-5.3.4 illustrate the flexural properties of cements containing EG-DMA referenced against the control TSBC for sample sets (n=5). 10EGMDA displayed a significantly higher ( $p<0.05$ ) maximum flexural strength (peak stress reached during plastic deformation, maximum value of Equation 4.5.1) than the control (0EGDMA), 2.5EGDMA, 20EGDMA and 25EGDMA. The sample sets 5EGDMA, 10EGDMA and 15EGDMA had significantly higher ( $p<0.05$ ) peak flexural strength than 2.5EGDMA, 20EGDMA and 25EGDMA. 5EGDMA and 15EGDMA had a significantly ( $p<0.05$ ) higher peak flexural strength than 2.5EGDMA, 20EGDMA and 25EGDMA (Figure 5.3.1). The maximum flexural strengths ranged from 114.84 MPa (10EGDMA) to 84.17 MPa (25EGDMA). The maximum flexural strength was also fit to a second-order polynomial with a measure of fit ( $R^2$ ) of 0.7442.

The bending modulus (Figure 5.3.3) (slope of the linear region of elastic deformation) was calculated using Equation 4.5.2 for all compositions within the elastic region of the stress vs. strain plots. There were no compositions with a significantly higher bending modulus ( $p<0.05$ ) than the control (2.8022 GPa), but 25EGDMA had a significantly ( $p<0.05$ ) lower bending modulus (2.4892 GPa). Samples containing 0-20 vol% had a significantly higher bending modulus than 25 vol% EG-DMA with the highest bending modulus occurring at 3.0431 GPa (10EGDMA). 5EGDMA, 10EGDMA and 15EGDMA had significantly higher ( $p<0.05$ ) bending moduli than 2.5EGDMA and 25EGDMA. The bending modulus was also fit to a second-order polynomial with an  $R^2$  value of 0.6928.



Figures 5.3.1-5.3.4: Maximum flexural strength (5.3.1), yield strength (5.3.2), bending modulus (5.3.3) and strain-to-failure (5.3.4) plotted as a function of EG-DMA vol%. Sample sets that are significantly different ( $p < 0.05$ ) are indicated by an asterisk (\*) and a line that spans between both sample sets. Bent lines with an asterisk indicate a grouping of significantly different sample sets.

The yield strength (Figure 5.3.2) was assessed at the point at which plastic deformation began (0.2% strain offset from elastic region) and elastic deformation ended. Plastic deformation is synonymous with non-recoverable deformation in the material (24). There were no significant differences between the control and samples containing 5-25 vol% EG-DMA, with 2.5 vol% EG-DMA samples being significantly weaker ( $p < 0.05$ ) than all other sample sets (46.87MPa). The highest measured yield strength for a sample set was at 15vol% EG-DMA (71.82 MPa).

There were no significant differences in the strain-to-failure data, however it should be noted that the test's limit was set at 10% strain (Figure 5.3.4). All of the control samples fractured before the upper threshold of the test and sample sets containing 2.5, 5, 20 and 25 vol% EG-DMA did not fracture. This would imply that those compositions have a higher average strain-to-failure limit than 10%. All EG-DMA samples exceeded ISO 5833:2002 Requirements for Bone Cements for bending modulus (minimum of 1.8 GPa) and maximum flexural strength (minimum of 50 MPa) (31). The mechanical properties of the control cement were similar to those previously reported in the Hasenwinkel lab (14).

#### *5.4 Conversion, exothermic heat, concentration of residual monomer and glass-transition temperature*

Figure 5.4.1 shows the different fractional monomer conversions for increasing concentrations of EG-DMA in the two-solution bone cement system. From Figure 5.4.1, it can clearly be seen that the control reaches the lowest conversion rate after 59 minutes with all compositions containing EG-DMA reaching higher levels of conversion. The isothermal test ran for 60 minutes; however, a negative heat flow was achieved after the first jump step (Table 4.6.1 and Figure A.1) and this data was removed and integration began once a positive heat flow (above 0 W/g) was recorded. Therefore, a full 60 minutes of data was not obtained for any composition and the nearest whole number was used

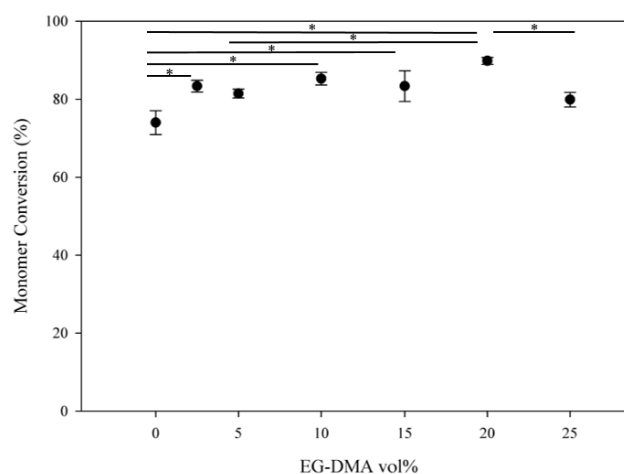


Figure 5.4.1: Fractional monomer conversion after being held 59 minutes isothermally. Groups connected with a line overhead and an asterisk (\*) are significantly different from one another ( $p < 0.05$ ).

for final conversion calculations across all samples (59 mins). Analyzing fractional conversion of monomer at 59 mins, there is a significant increase ( $p < 0.05$ ) in conversion for samples containing 2.5 vol%, 10 vol%, 15 vol% and 20 vol% EG-DMA from the control with a peak conversion at 20 vol% EG-DMA (89.81%). The lowest conversion of the EG-DMA samples occurred at 79.88% (25EGDMA), also higher than the control (73.98%). 20EGDMA was significantly ( $p < 0.05$ ) higher than the control, 5EGDMA and 25EGDMA. Looking at Figure 5.4.5 and A.1, it would appear that the initial curing reaction happens within the first 10 minutes with the remaining 50 minutes accounting for less than 10% of the samples conversion. The heat of reaction (Figure 5.4.2) for all compositions containing EG-DMA was significantly higher ( $p < 0.05$ ) than the control. 20EGDMA had a significantly higher heat of reaction than 2.5EGDMA, 5EGDMA and 25EGDMA. The concentration of residual monomer is directly related to the fractional monomer conversion.

2.5EGDMA, 10EGDMA, 15EGDMA and 20EGDMA samples had significantly less ( $p < 0.05$ ) residual monomer (Figure 5.4.3) than the control (26.02%) with 20EGDMA (10.19%) having the least amount of residual monomer of the samples containing EG-DMA. 25EGDMA and 5EGDMA had lower residual monomer concentrations than the control, but not to a significant effect ( $p < 0.05$ ). The control sample's fractional conversion and residual

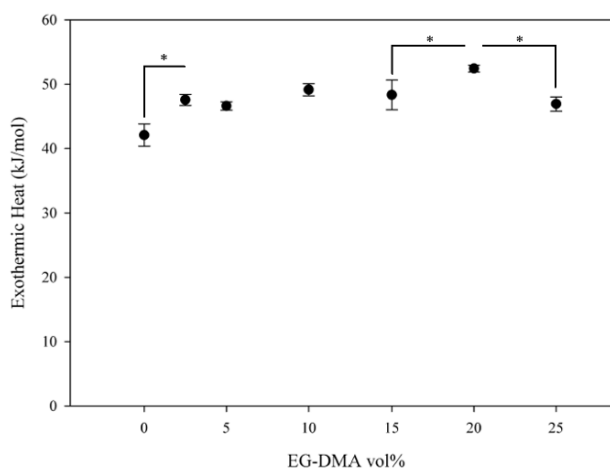
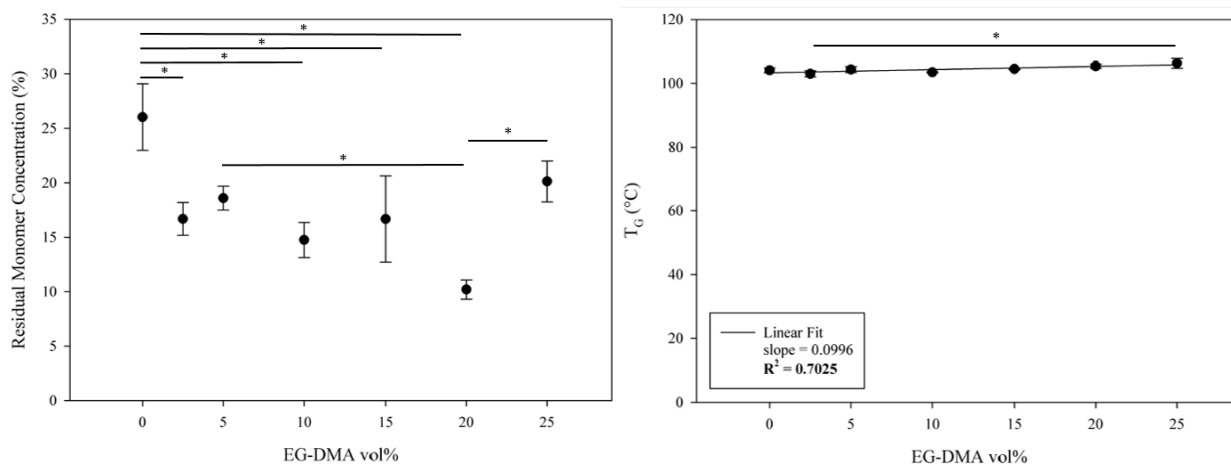


Figure 5.4.2: Exothermic heat of reaction as a function of EG-DMA vol%. Groups connected with a line overhead and an asterisk (\*) are significantly different from one another ( $p < 0.05$ ). Bent lines signify a grouping of compositions.



monomer concentration were consistent with previously reported data in the Hasenwinkel lab (14). The glass-transition temperature (Figure 5.4.4) was measured using the second non-isothermal scan of the material after all residual monomer had been driven to conversion (Figure A.2). There was no significant difference ( $p < 0.05$ ) between samples containing EG-DMA and the control. There was a significant increase ( $p < 0.05$ ) in the glass-transition temperature between 2.5EGDMA and 25EGDMA, and glass-transition temperature showed a positive correlation with increasing EG-DMA content. Crosslinking has been shown to increase the glass-transition temperature in polymeric materials (24) and this could indicate an increase in crosslinking between polymerized samples containing EG-DMA. Figure A.1 displays heat flow vs. time for the duration of the experiment using the control TSBC with the different sections of the method file labeled. Figure 5.4.5 displays the fractional monomer conversion data for all formulations.



Figures 5.4.3-5.4.4: Residual monomer concentration (5.4.3) and glass-transition temperature (5.4.4) plotted as a function of EG-DMA vol%. Sample sets that are significantly different ( $p < 0.05$ ) are indicated by an asterisk (\*) and a line that spans between both sample sets.

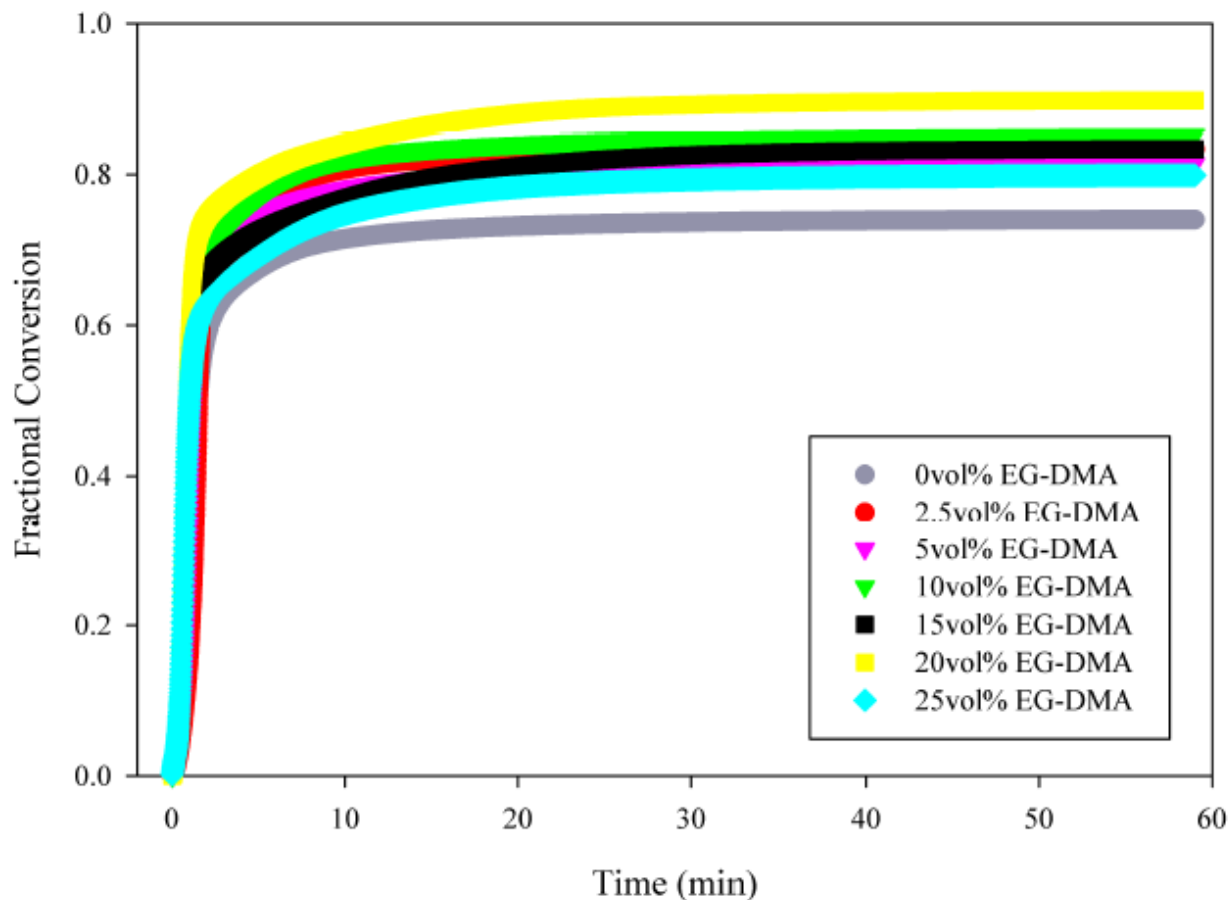


Figure 5.4.5: Fractional conversion of all compositions during the isothermal DSC experiment. The control resulted in the lowest amount of fractional monomer conversion and 20 vol% EG-DMA produced the highest fractional conversion after 59 minutes.

### 5.5 Viscosity analysis

Viscosity measurements were taken across all shear rates that were measurable in triplicate for each composition. Measurements were recorded 10 times across 5 minutes, every 30 seconds after viscosity stabilization. When switching between shear rates, the material needed time to stabilize at the new RPM before accurate readings could be taken. This was signaled when the viscometer stopped blinking. The DV-E rheometer recorded torque in addition to viscosity, and torque increased with increasing shear rates. Readings were recorded after the torque measured above 10% and ceased once the viscosity and torque readings measured “EEEE cP” and “EEEE

%” respectively. This was representative of torque over 100%. There was only one shear rate ( $0.8 \text{ s}^{-1}$ ) where all compositions were recordable. The control composition didn’t produce enough torque for accurate readings below this shear rate, and 25 vol% EG-DMA produced torque greater than 100% (EEEE %) above this shear rate. At a shear rate of  $0.8 \text{ s}^{-1}$ , compositions containing 5-25 vol% EG-DMA were significantly higher ( $p < 0.05$ ) in viscosity than the control. 25EGDMA had a significantly higher ( $p < 0.05$ ) viscosity than all other samples, 20 EGDMA had a significantly ( $p < 0.05$ ) higher viscosity than 2.5EGDMA, 5EGDMA, 15EGDMA and the control. 10EGDMA had a significantly higher ( $p < 0.05$ ) than 2.5EGDMA, 15EGDMA and the control. 15EGDMA and 5EGDMA were significantly higher ( $p < 0.05$ ) than 2.5EGDMA and the control (Figure 5.5.1). Compositions 2.5-20 vol% EG-DMA all had viscosities significantly higher ( $p < 0.05$ ) than the control for shear rates greater than  $0.8 \text{ s}^{-1}$  ( $1, 1.2, 1.6, 2, 2.4 \text{ s}^{-1}$ ). 25EGDMA was significantly higher ( $p < 0.05$ ) than all other concentrations at all measurable shear rates. At higher shear rates ( $2 \text{ s}^{-1}, 2.4 \text{ s}^{-1}$ ), 20EGDMA had a significantly higher ( $p < 0.05$ )

viscosity than all other measurable concentrations. Across all shear rates, 2.5EGDMA is significantly lower in viscosity ( $p < 0.05$ ) than all other EG-DMA compositions. For all shear rates it followed the basic correlation that the higher the EG-DMA concentration, the higher the measured viscosity (Figures 5.5.2-5.5.9) with a few

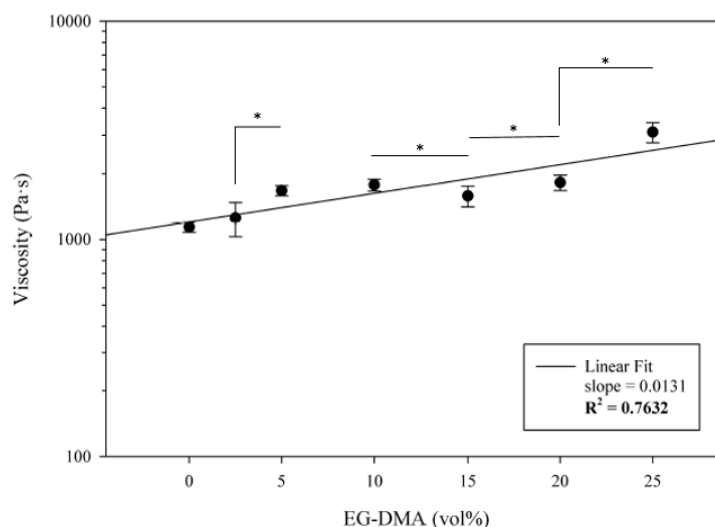


Figure 5.5.1: Viscosity measurements as a function of EG-DMA vol% at a fixed shear rate of  $0.8 \text{ (1/s)}$ . Groups connected with a line overhead and an asterisk (\*) are significantly different from one another ( $p < 0.05$ ). Bent lines signify a grouping of compositions.

exceptions. For example at  $0.4 \text{ s}^{-1}$ , 2.5EGDMA and 15EGDMA are significantly lower ( $p < 0.05$ ) in viscosity than all other EG-DMA containing compositions. At  $0.4 \text{ s}^{-1}$ , 5EGDMA is significantly ( $p < 0.05$ ) higher than 20EGDMA. Excluding the few exceptions, these relationships can be inferred because PMMA beads do not dissolve in EG-DMA, and therefore the PMMA to MMA ratio increases with increasing EG-DMA concentrations. The increase in density of the

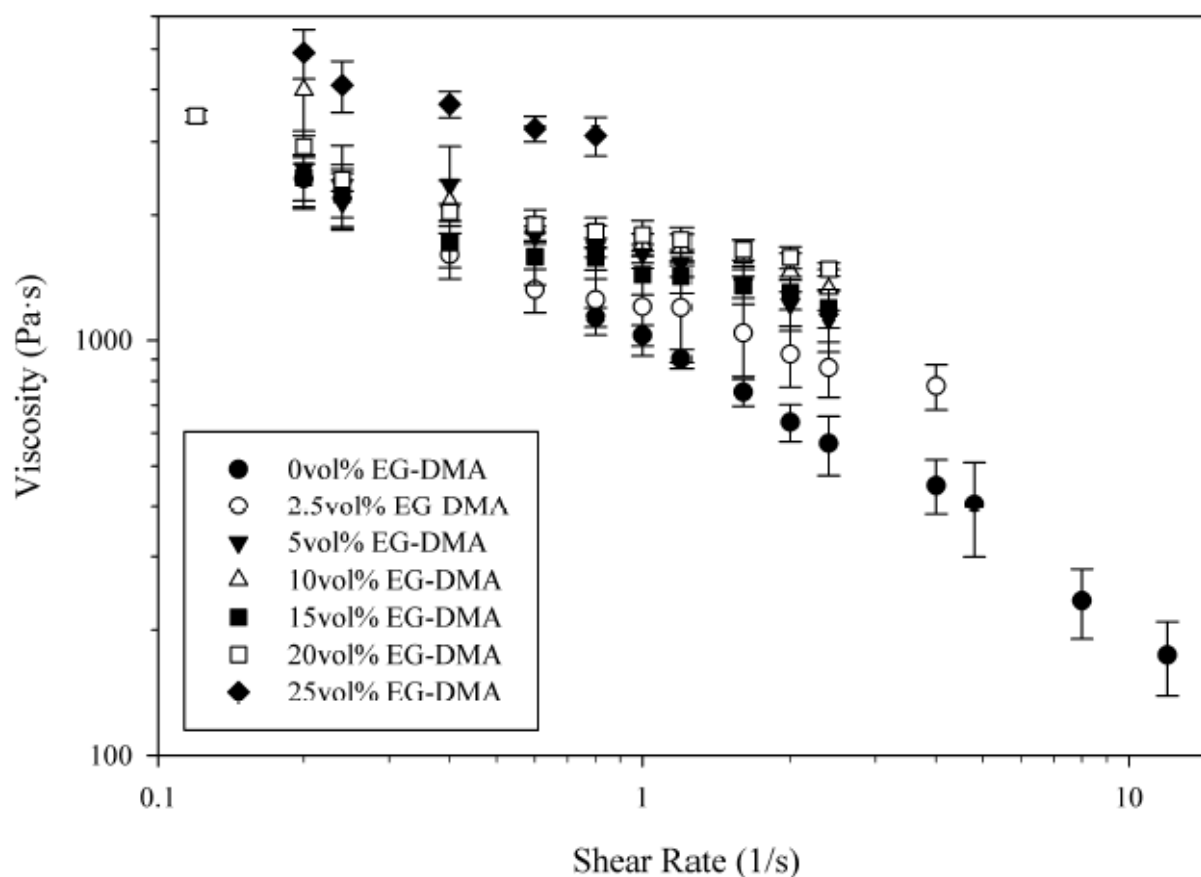


Figure 5.5.2: Viscosity profiles for each composition across all recordable shear rates. Each shear rate was tested in triplicate.

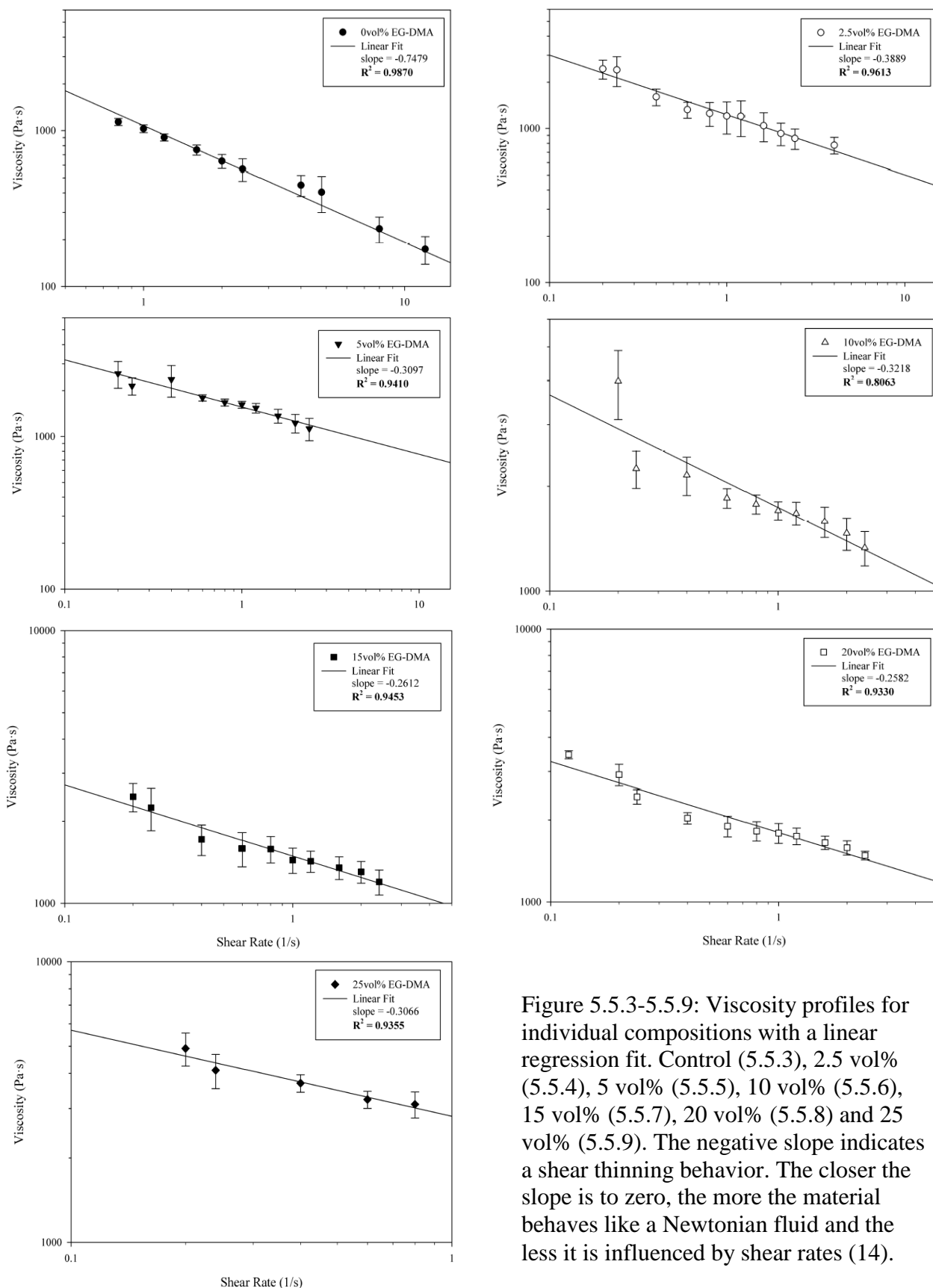


Figure 5.5.3-5.5.9: Viscosity profiles for individual compositions with a linear regression fit. Control (5.5.3), 2.5 vol% (5.5.4), 5 vol% (5.5.5), 10 vol% (5.5.6), 15 vol% (5.5.7), 20 vol% (5.5.8) and 25 vol% (5.5.9). The negative slope indicates a shear thinning behavior. The closer the slope is to zero, the more the material behaves like a Newtonian fluid and the less it is influenced by shear rates (14).

PMMA/MMA slurry decreases the ability of the material to be deformed and flow freely. Replacing equal volumes of MMA (0.94 g/mL) with EG-DMA (1.051 g/mL) will increase the viscosity of the resulting material. All viscosities were plotted on logarithmic-logarithmic scale and fitted to a linear regression. The slopes of the regression lines in Figures 5.5.3-5.5.9 give the type and degree of non-Newtonian flow, in which a zero slope would indicate Newtonian behavior (14). All the slopes reported are negative signifying shear thinning behavior for all compositions tested. While the control cement was significantly lower in viscosity ( $p < 0.05$ ) at all shear rates than samples containing 5-25 vol% EG-DMA, it did have a more negative slope demonstrating more pseudoplasticity (14). This would imply that the EG-DMA samples are less sensitive to shearing forces. The viscosities reported for the control cement were similar to those previously reported in the Hasenwinkel lab (14).

#### *5.6 Scanning electron microscopy and optical imaging*

SEM micrographs (Figures 5.6.1-5.6.3) revealed a ripple deformation along the fracture surface in samples containing EG-DMA, indicating a change in the plastic deformation mechanism in comparison to the control. The control sample micrographs contained concentric artifacts that originated from one fracture point, representing the site of crack formation and subsequent propagation. These morphologies are consistent with those previously reported (3).

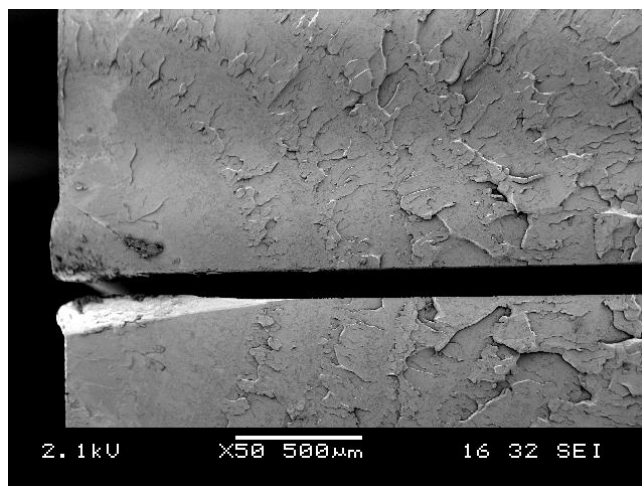
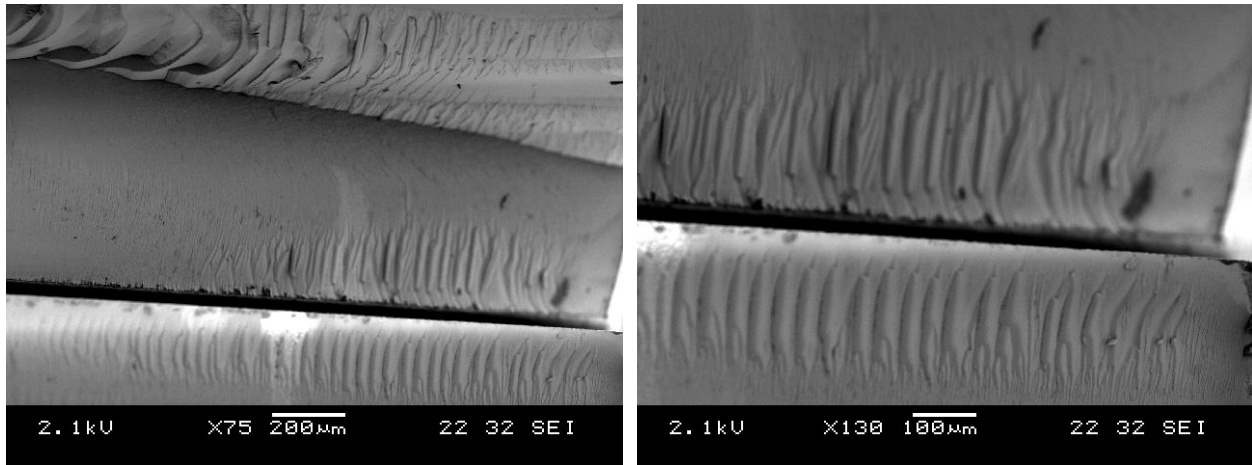
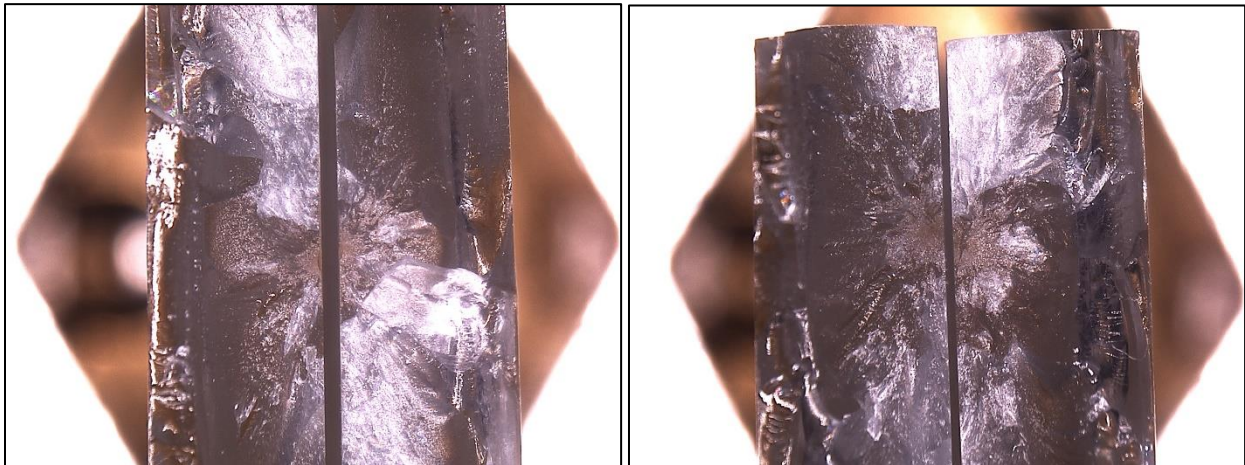


Figure 5.6.1: SEM micrograph of the control sample fracture site during three-point bend tests. Notice the concentric rings that originate from the point of failure. The smooth surface between the rings represents a fast fracture mechanism.



Figures 5.6.2-5.6.3: Cement containing 25 vol% EG-DMA, fractured from three point bend tests. Observe the ripple formation along the fracture edge that is present in the above micrographs, but absent from control samples. It is believed this is a result of the plastic deformation mechanism and higher strain-to-failure values.

This phenomenon is less prominent in EG-DMA samples with a rippled ridge along the fracture surface more visible. These morphological changes could be a direct result of the substitution of MMA for EG-DMA, causing a change in the bond stretching and deformation (15). Imaging using the high magnification optical microscope revealed a uniformity in these morphological changes across the entire fracture surface. A different fracture pattern than the control was



Figures 5.6.4-5.6.5: Digital optical images of TSBC fracture surfaces with 10 vol% EG-DMA. The point of fracture and surface is different than the control samples (Figures B.3-B.4). It should also be noted that these samples fractured into several pieces whereas the control samples fractured into two pieces.

observed (Figures 5.6.4-5.6.5) once the surface was imaged at lower magnifications. These images revealed a larger scale version of the ridges seen in the SEM micrographs originating from the point of fracture as well as along the edge of the sample. Also, where the surfaces of the control samples were relatively flat, the EG-DMA samples produced surfaces with many protruding edges and points. Additional SEM micrographs and supplementary optical imaging pictures can be found in Appendix B.

## 6. Discussion

Substitution of methyl methacrylate (MMA) monomer for ethylene glycol-dimethacrylate (EG-DMA) crosslinker was observed to increase viscosity of the two-solution formulation while improving thermal and mechanical characteristics for certain concentrations of EG-DMA. These compositions appear to improve upon some of the setbacks of commercial cements for the treatment of implant augmentation and fixation. The higher viscosity in the modified TSBCs containing EG-DMA can be attributed to a higher PMMA to MMA ratio, increasing the resistance to flow and deformation. Improved mechanical properties of the modified TSBCs can be credited to EG-DMA crosslinks between adjacent PMMA chains in the polymerized sample.

The effect of EG-DMA on exothermal and setting properties at increasing concentrations of EG-DMA was evaluated using the standard ASTM F451 mold (25). As previously mentioned, there was no significant difference ( $p < 0.05$ ) in the maximum polymerization temperature between the control TSBC and the modified compositions. This could be expected because there are off-setting variables with increasing EG-DMA content. Referencing Table 4.1.1, the moles of monomer decreased with increasing EG-DMA content but the available double bonds present for free radical polymerization increased. EG-DMA molecules are larger in molecular weight and



density than MMA molecules, therefore, replacing MMA molecules with the larger EG-DMA molecules occupying the same volume gives lower total moles. The amount of double bonds slightly increases because although EG-DMA molecules are almost twice as large as MMA molecules, 198.22 g/mol to 100.121 g/mol respectively, EG-DMA has twice as many double bonds. Thus, EG-DMA contains slightly more double bonds per unit mass, and by referencing the density, per unit volume as well. Replacing the same volume of MMA with EG-DMA gives a slight increase in total number of double bonds present. We expected polymerization temperatures and heat generated to remain consistent across samples because while decreasing the moles present would decrease the overall heat generated, increasing the amount of double bonds would increase the overall heat generated. All samples had a significantly ( $p < 0.05$ ) higher heat of reaction and these changes could be attributed to the high reactivity of EG-DMA molecules, as previously mentioned by Zuk et al. (22). The increased heat of reaction can help explain the significant differences in polymerization conversion achieved by EG-DMA samples. The heat of reaction is directly related to the number of MMA and EG-DMA carbon-carbon double bonds broken, therefore the more heat released, the higher the conversion rate.

It was determined that samples containing 2.5-20 vol% EG-DMA had a significantly higher ( $p < 0.05$ ) conversion rate with a significantly ( $p < 0.05$ ) lower residual monomer concentration after 59 minutes of isothermal-DSC. This further (22) confirms that the EG-DMA molecules are more reactive than MMA molecules in this environment. The amount of the double bonds present in the highest concentration of EG-DMA (25 vol%) is only 3% higher than the control TSBC. The conversion rates measured are much higher than a 3% increase for EG-DMA samples, indicating that the EG-DMA molecules are more reactive than the MMA monomer molecules. It should be noted again that the heat released by a carbon-carbon double bond in an

MMA molecule is indistinguishable from an EG-DMA molecule, and thus the conversion was taken as a percentage of all monomer molecules theoretically present (18).

Viscometry tests were performed at every measurable shear rate across all compositions. There was an observable trend across the compositions that as EG-DMA concentration increased, so did the viscosity at any given shear rate. This was expected due to the substitution of MMA for EG-DMA. EG-DMA has a higher viscosity than MMA, and PMMA resin is not soluble in EG-DMA monomer. Therefore, the PMMA/MMA slurry density increased with EG-DMA content and the resulting mixtures had significantly ( $p < 0.05$ ) greater viscosities. The EG-DMA compositions have a more stable viscosity across all shear rates (slope of the regression line) which allows for a consistent application of the material no matter the applied pressure. This is commercially advantageous over other high viscosity cements because of its consistency, creating less variation between samples and applications (2, 5).

The mechanical properties of the EG-DMA samples were either significantly equivalent ( $p < 0.05$ ) or superior to the TSBC control for maximum flexural strength, bending modulus, yield strength, and fracture toughness, depending on the composition. Some compositions displayed a ‘drop-off’ in mechanical integrity past a certain concentration of EG-DMA. Increasing the amount of monomer available has been proven to increase the probability of longer polymerized chains and higher molecular weights in the set cement (3), and higher molecular weight polymers have been proven to possess superior mechanical properties than lower molecular weight polymers (24).

The maximum flexural strength (Figure 5.3.1) increased with increasing EG-DMA content up to 10 vol% before the strength decreased. This trend follows a second order polynomial with an  $R^2$  value of 0.7442. This would indicate that up to 10 vol%, the EG-DMA crosslinker has more of an effect on the strength of the material than the decreasing MMA content. After 10 vol%,

decreasing the amount of MMA available appears to dominate mechanical properties regardless of crosslinker concentration. The bending modulus increases with increasing EG-DMA content up to 10 vol% and then decreases with increasing EG-DMA concentrations. The bending modulus follows a similar polynomial trend as seen in the maximum flexural strength data with an  $R^2$  value of 0.6929. The yield strength has less of a noticeable trend with increasing EG-DMA content. Yield strength increased up to 15 vol% EG-DMA, then decreased at 20 vol% and recovered some strength at 25 vol% EG-DMA.

During fracture toughness tests, the  $K_{IC}$  increased with increasing EG-DMA content up to 5 vol% EG-DMA at about  $1.6 \text{ MPa}\cdot\text{m}^{1/2}$  but then significantly fell off at 10 vol% to below  $0.8 \text{ MPa}\cdot\text{m}^{1/2}$  and decreased exponentially after that up to the maximum EG-DMA concentration of 25 vol%. We predicted the fracture toughness of the material to increase with increasing crosslinker content, however similar to other mechanical properties, decreasing MMA content dominates the crosslinker effect at a certain point. Deb et al. (10) reported that mechanical properties of acrylic bone cements based on poly(ethylmethacrylate)-*n*-butylmethacrylate (PEMA) improve with the addition of crosslinking agents such as EG-DMA and triethylene glycol-dimethacrylate (TEG-DMA) at low concentrations (2.5-5 wt/wt %) but steadily decrease when the concentrations are increased. Yang et al (19) reported similar mechanical trends using tricalcium phosphate (TCP), HEMA and EG-DMA within an acrylic bone cement system. We attribute these similar trends to molecular-level changes within the material. Weak van der Waal's forces within the PMMA matrix are being replaced with stronger physical covalent bonds as crosslinking increases. At higher crosslinker concentrations, 'submicro cracks' (19) develop within the material caused by internal stresses as a result of shrinkage or thermal changes (32). These micro cracks are then observed in post hoc SEM imaging (Figure 6.1). The rougher EG-

DMA surfaces are due to the crack front interacting with a greater number of micro cracks within the material. These interactions cause crack arrest or out-of-plane crack deflection. This results in larger fracture surface area and micro craters/volumes where mode I opening does not apply (33), both of which increase  $K_{IC}$  values. Lednicky and Pelzbauer (34) proposed that PMMA based cements undergo a coalescence fracture mechanism between primary and secondary crack fronts. The secondary crack fronts are initiated at the micro volumes within the material and when the secondary crack front meets the primary crack front, the fracture mechanism increases in speed and decreases in magnitude. This is in agreement with the higher concentrated EG-DMA samples tested.

SEM micrographs confirmed a different fracture mechanism presented in the EG-DMA samples. During three-point bend tests, fractured TSBC fragments produced two pieces with mirrored

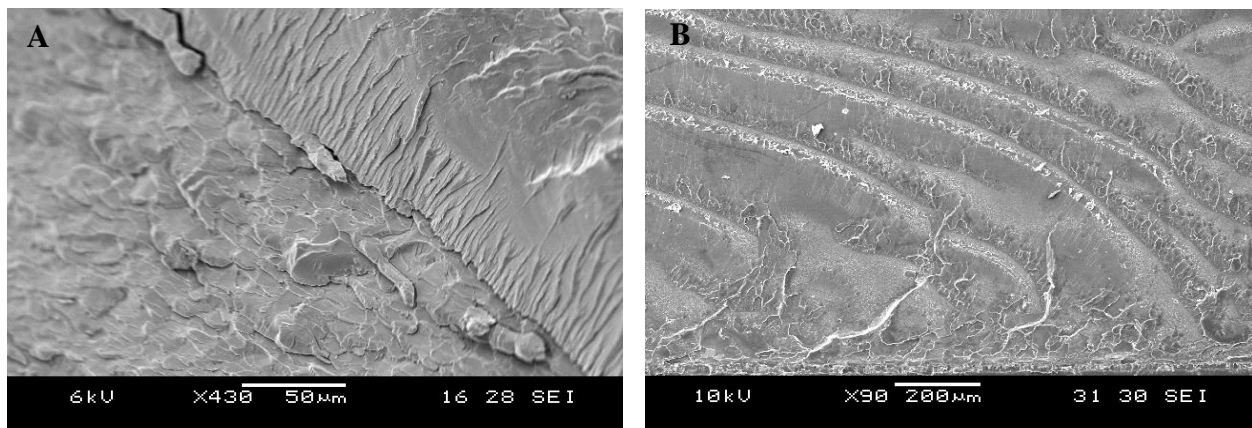


Figure 6.1: Micrographs of a three-point bend sample (A) and fracture toughness sample (B) displaying high magnified fractured surfaces. (A) 10EGDMA and (B) 2.5EGDMA samples display rough surfaces with micro cracks, ridges and small craters along the surface

fracture surfaces. The EG-DMA samples that broke fractured in more than two pieces with varying fracture surfaces and morphology. The TSBC fracture surface was characterized by concentric elliptical zones originating from the bottom surface subjected to tension. The crack continues to propagate radially until it reaches the other edge subjected to compression from the

crosshead. EG-DMA samples contained several small ridges or “tufts” (10  $\mu\text{m}$  wide) and little craters along the fracture surface that are indicative of high levels of plastic deformation (Figure 6.2). This indicates that the PMMA was subjected to large amounts of plastic strain before failure (32). EG-DMA samples had higher strain-to-failure values and by association, larger plastic deformation regions than the TSBC control. This conforms with Min et al.’s molecular dynamic simulations that crosslinking PMMA chains with EG-DMA molecules increases the ductility due to the increased alignment and resistance to deformation along the carbon backbone (15).

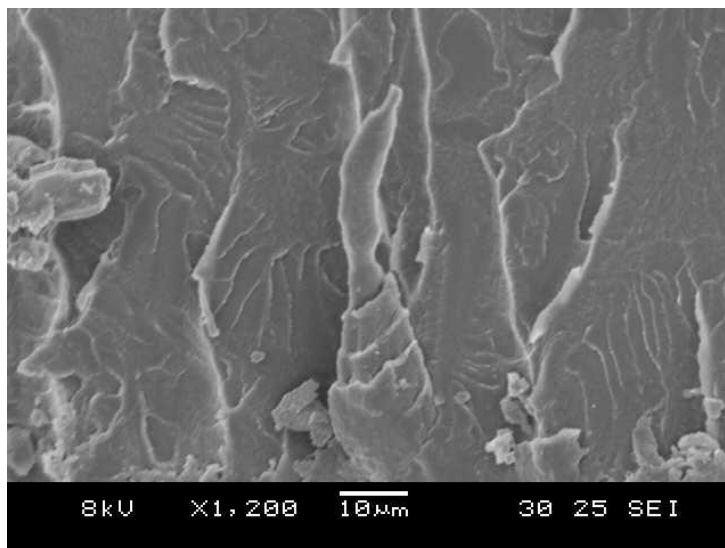


Figure 6.2: SEM micrograph of 5 vol% EG-DMA at 1,200X magnification of the fracture edge. Micro troughs are visible along the boundary of the fracture surface (Three-point bend sample).

## 7. Conclusion

The results presented in this work demonstrate the thermal, mechanical & viscous properties of crosslinked two-solution bone cement formulations. Certain compositions provided superior mechanical integrity while others demonstrated improved monomer conversion or lower exothermal properties. Samples containing 5-10 vol% EG-DMA demonstrated the greatest improvement in mechanical properties, while those with 15-20 vol% had the highest levels of monomer conversion with the lowest amount of residual monomer. Sample sets containing 2.5, 5, 20 and 25 vol% EG-DMA did not fracture during three-point bend tests, indicating an increase in ductility from the control TSBC. 5EGDMA had the largest fracture toughness, 10EGDMA

had the greatest maximum flexural strength and bending modulus. 15EGDMA had the highest yield strength, and 20EGDMA had the highest level of monomer conversion. Samples containing 25 vol% EG-DMA had significantly lower polymerization temperatures while all compositions produced a significantly greater amount of heat during the initial polymerization. All modified samples expressed an increase in viscosity, with a positive correlation between increasing EG-DMA content and increasing viscosity. 5EGDMA and 10EGDMA would be the best candidates for an alternative solution used in load bearing applications like total arthroplasties of the lower extremities due to their superior mechanical integrity when compared to the control TSBC. For uses that require minimalization of residual monomer, 20EGDMA is the most suitable formulation. One possible use could be vertebroplasty where reducing the amount of monomer in the cured sample contributes to pain relief (13). Overall, EG-DMA proved to have an appreciable effect on the characterization of the TSBC.

## **8. Future Work**

The results presented in this work provide a detailed characterization involving the substitution of MMA for EG-DMA. A continuation of this work would include compositions with 5-20 vol% EG-DMA as these formulations demonstrated improvement in mechanical and thermal properties. There have been recent attempts to modify PMMA based cements with biodegradable polymers and osteoconductive bioceramics for fracture fixation and bone regeneration. We believe that the EG-DMA formulations will provide a good platform for future work involving these materials for similar purposes.

Poly(DL-lactic-*co*-glycolic acid) (PLGA) is a synthetic copolymer that degrades by nonenzymatical hydrolysis of the carbon-backbone ester linkages (35, 36). It has been found that

the incorporation of PLGA in PMMA/MMA bone cements can create controlled porosity via bulk and surface degradation of the PLGA microsphere constituent (37). Additionally, PLGA degradation in calcium phosphate/PLGA scaffolds did not generate an immune response after 12 weeks *in vivo* and histomorphometric analysis confirmed new bone deposition within degraded scaffolds (36). It has also been found experimentally in the Hasenwinkel lab that PLGA is soluble up to 200 wt% (g/mL) in MMA. This is an attractive feature because by adding greater concentrations of polymer to the monomer solution, we are reducing the amount of PMMA in the final cured sample. This reduces the amount of material that cannot be degraded.

Calcium sulfate is also an osteoconductive radiopaque inorganic material with faster (4 weeks) degradation characteristics than calcium phosphate (1 year) (39). Calcium phosphate and calcium sulfate cements are known to be brittle, and recent attempts have been made to incorporate these radiopaque additives with acrylic based cements (40). Barium sulfate, a crystalline inorganic radiopaque material, when added to Simplex cement decreases the ultimate tensile strength and fracture toughness of the cured cement (40). Deb et al. (32) added barium sulfate particulate to acrylic bone cement containing small amounts of methacrylate-based crosslinker and showed an increase in tensile strength and ductility. This was attributed to the barium sulfate acting as a filler in the more flexible crosslinked network. We hypothesize that the addition of PLGA and calcium sulfate in the EG-DMA modified cement formulations will provide a similar effect as described (32, 40).

## Appendix A- DSC output file

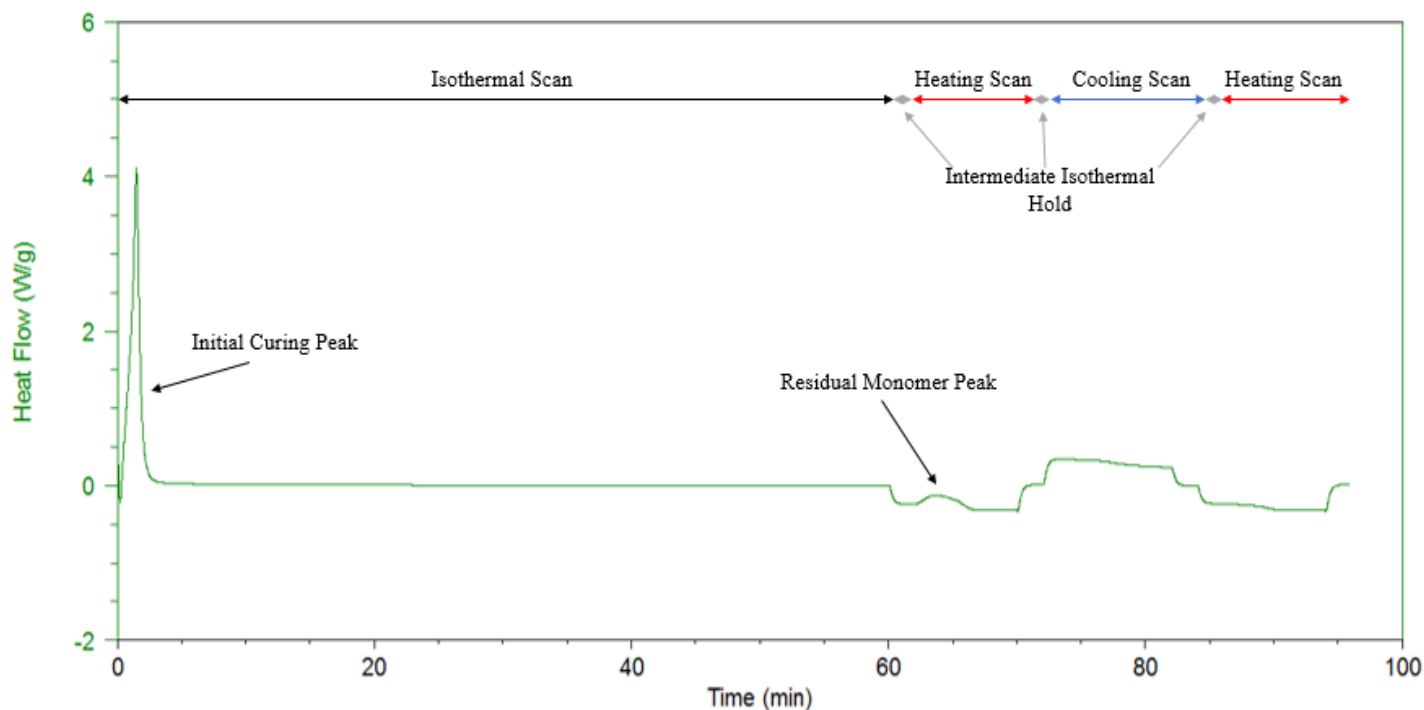


Figure A.1: DSC exotherm of the TSBC control. Isothermal and non-isothermal stages are marked as well as the initial curing peak and residual monomer peak. Notice the lack of residual monomer peak in the second heating scan.

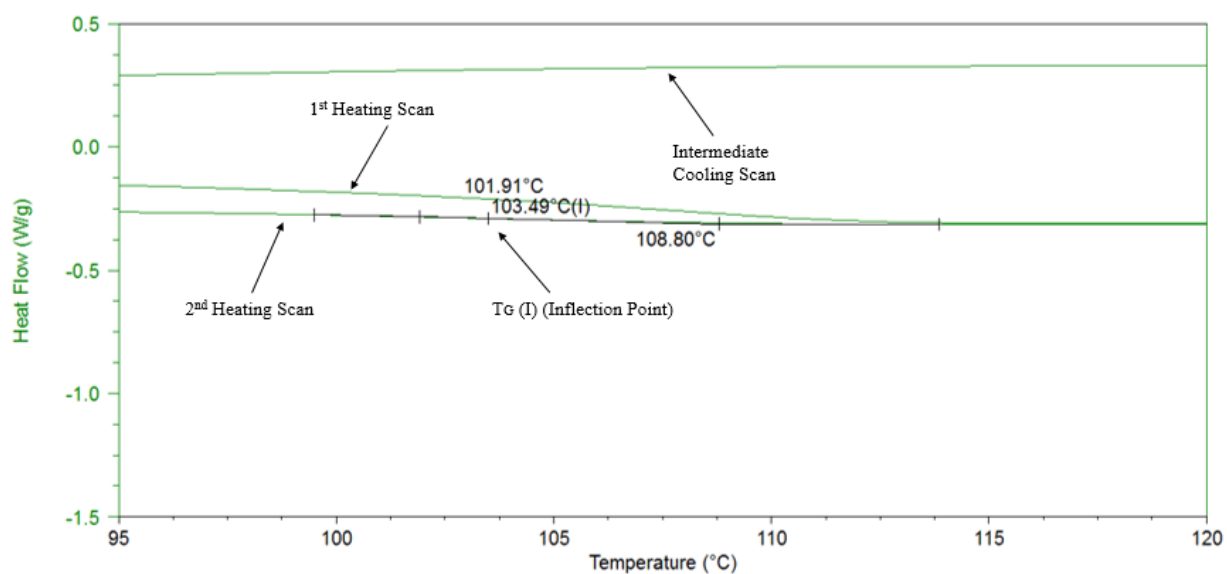
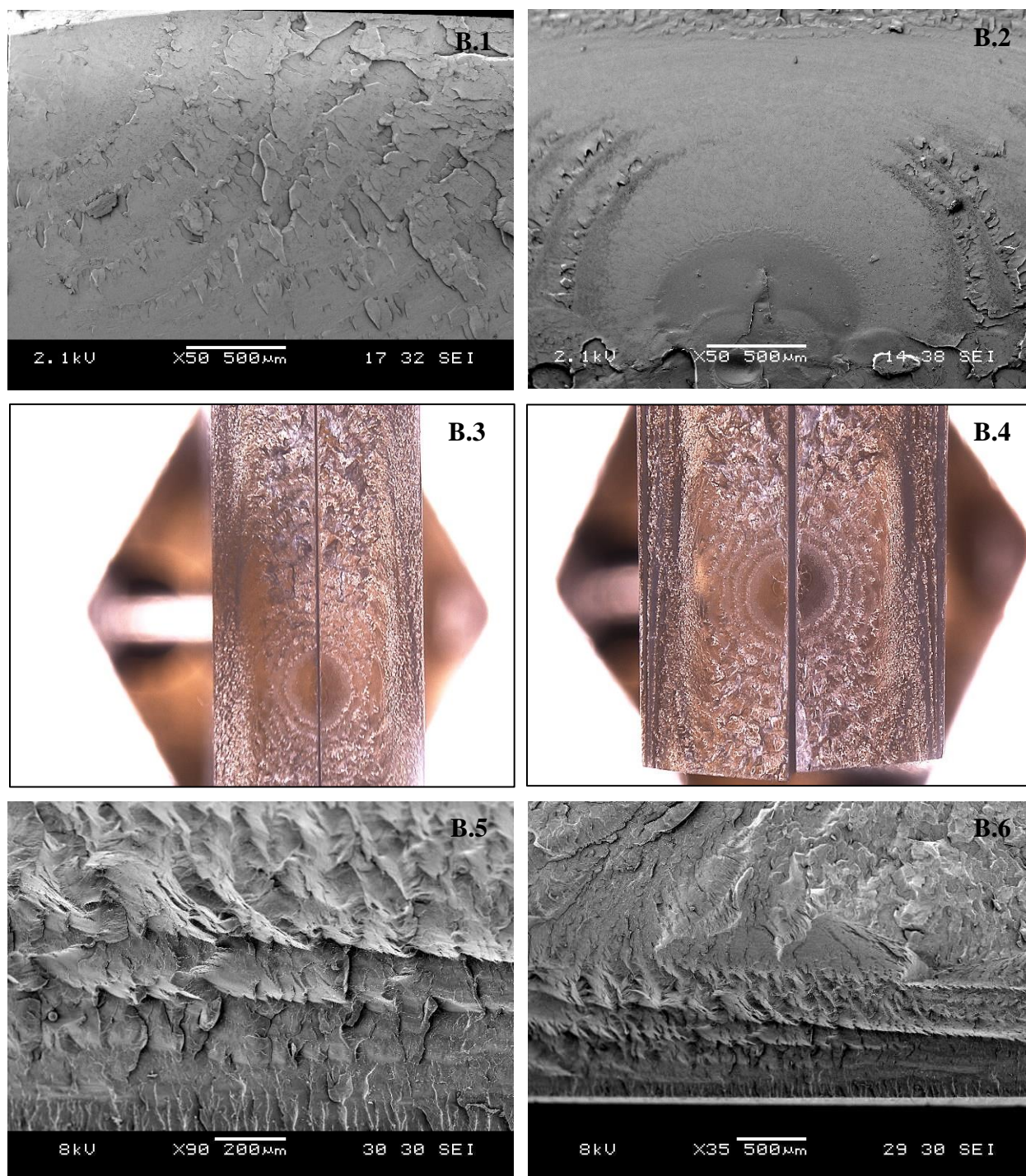


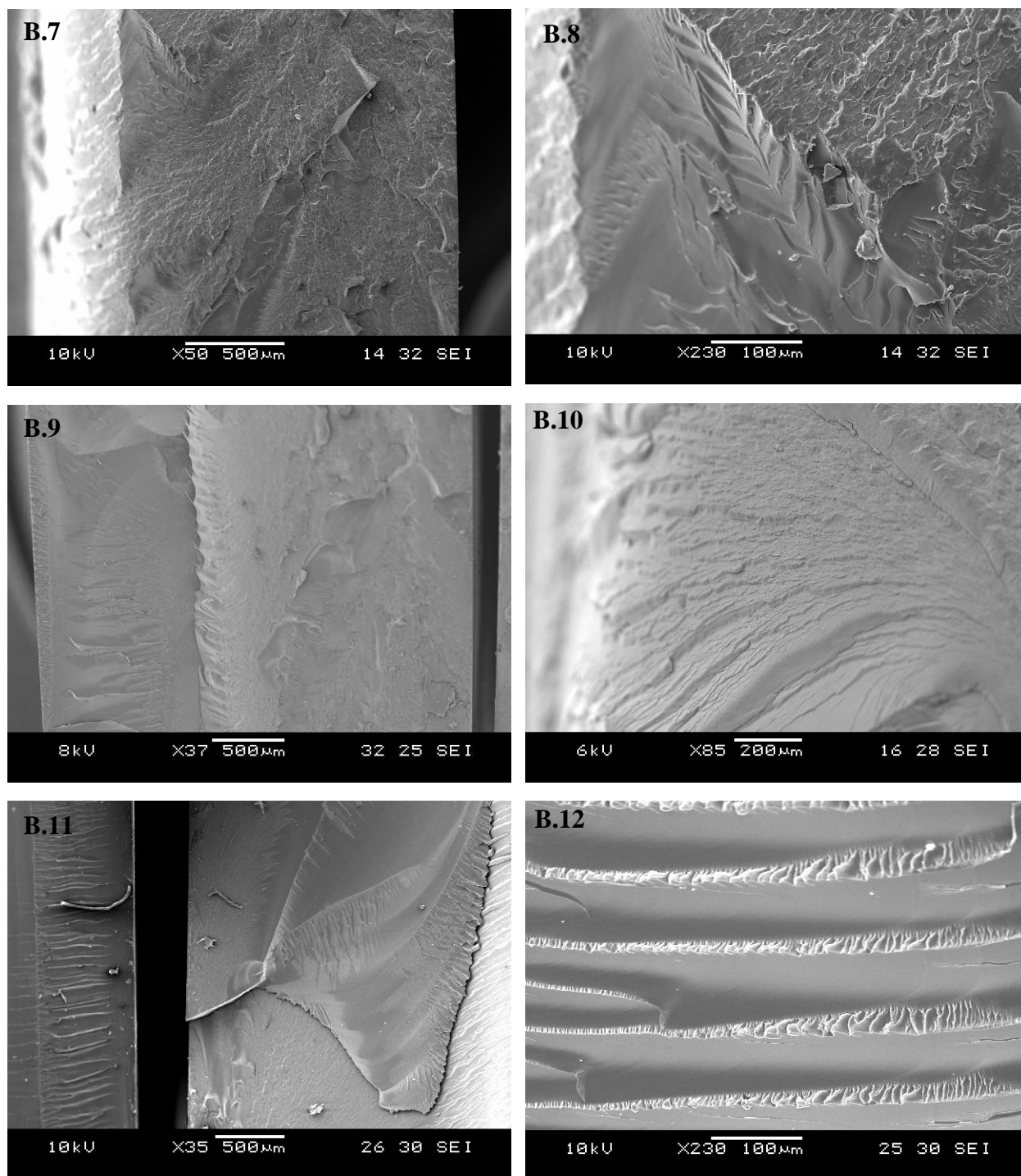
Figure A.2: Heat flow vs. temperature for the control TSBC. The glass-transition temperature was measured using the inflection point during the second heating scan. DSC exotherms confirmed the absence of the residual monomer peak, making the glass-transition temperature measurement possible.



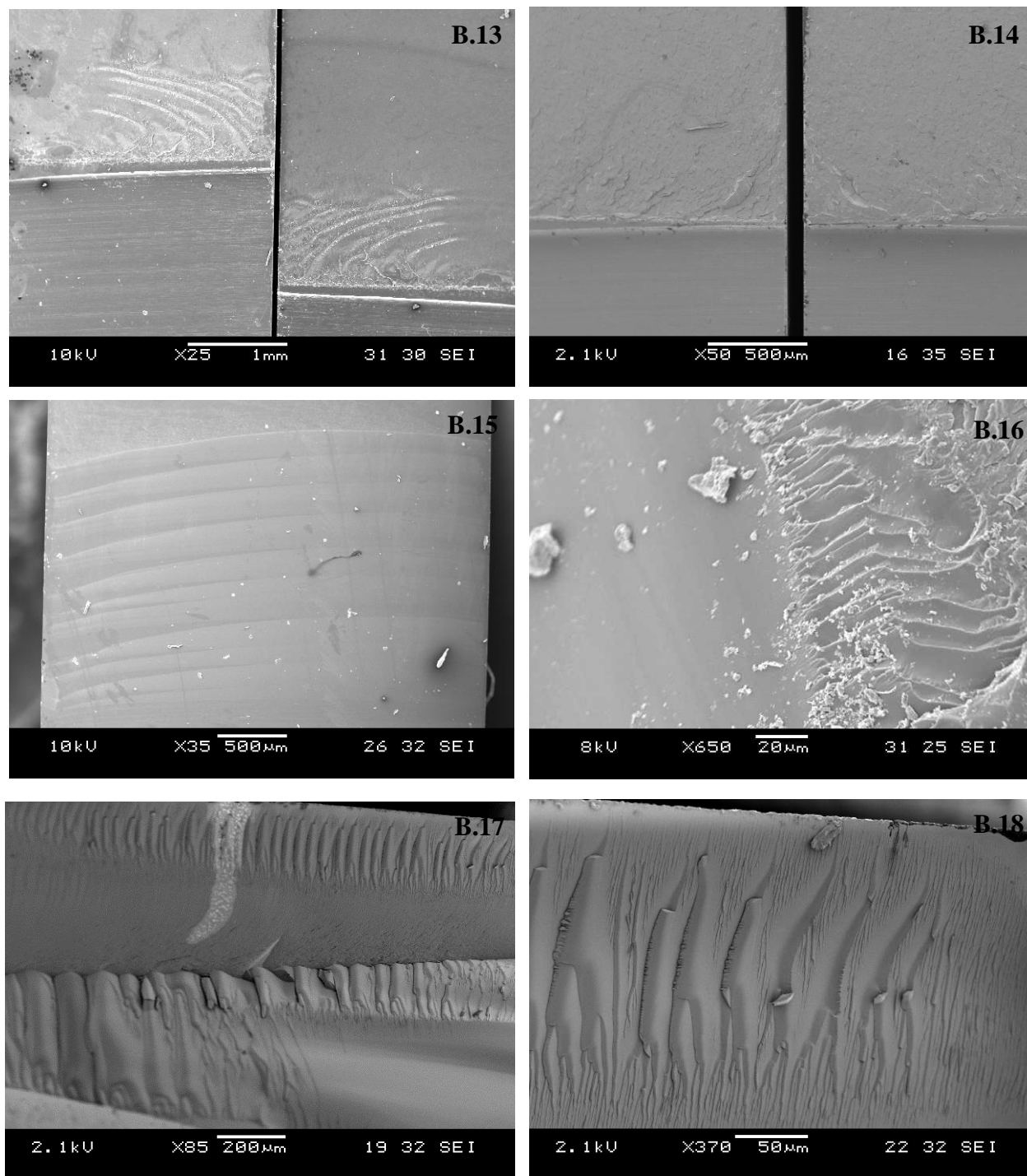
## Appendix B- SEM and digital optical microscope images



Figures B.1-B.6: Fracture surfaces of the TSBC control (B.1, B.2) showing the concentric rings originating from the fracture surface. Digital optical images of the control sample immediately after fracture (B.3, B.4). B.5 and B.6 are high magnification images of the fracture surface of a sample containing 5 vol% EG-DMA. There are micro-scaled ridges and microcracks as a direct result of plastic deformation.



Figures B.7-B.12: Three-point bend fracture surfaces of TSBC with 10 vol% EG-DMA (B.7, B.8), 15 vol% EG-DMA (B.9, B.10) and 20 vol% EG-DMA (B.11, B.12). Ridges as a result of plastic strain and deformation (B.9, B.11) of 15EGDMA. Zoomed in micro-ruffles (B.12) of the same sample.



Figures B.13-B.18: Fracture toughness test surfaces of the TSBC with 2.5 vol% EG-DMA (B.13), 5 vol% EG-DMA (B.14) and 20 vol% EG-DMA (B.15). Ridges as a result of plastic strain and deformation of 15EGDMA (B.16). Zoomed in micro-ruffles of the same sample. B.17 displays the micro-craters along the fracture surface in 25EGDMA. The fracture surface edge (B.18) of a fractured 25EGDMA sample.



### Appendix C- Experimental data for all experiments with standard deviations (SD)

**Table C.1: Exothermal and mechanical properties of TSBCs modified with EG-DMA**

	Control	2.5EGDMA	5EGDMA	10EGDMA	15EGDMA	20EGDMA	25EGDMA
Maximum polymerization temperature (°C)	83.43 (2.25)	77.59 (3.36)	88.74 (5.09)	83.26 (9.79)	92.56 (3.24)	91.67 (4.85)	73.21 (2.58)
Setting time (min)	5.23 (0.38)	5.31 (0.26)	4.64 (0.07)	4.72 (0.47)	4.92 (0.24)	5.43 (0.15)	4.75 (0.36)
Strain-to-failure (%)	7.62 (2.04)	10 (0)	10 (0)	9.01 (1.97)	8.78 (1.51)	10 (0)	10 (0)
Fracture toughness (MPa*m <sup>1/2</sup> )	1.3588 (0.08)	1.433 (0.27)	1.6055 (0.18)	0.7800 (0.07)	0.4239 (0.06)	0.3092 (0.02)	0.2584 (0.06)
Maximum flexural strength (MPa)	97.86 (5.09)	90.01 (4.30)	110.31 (11.70)	114.84 (8.77)	108.26 (6.35)	93.25 (6.25)	84.17 (3.33)
Bending modulus (GPa)	2.80 (0.10)	2.57 (0.09)	2.90 (0.22)	3.04 (0.16)	2.93 (0.13)	2.81 (0.14)	2.49 (0.11)
Yield strength (MPa)	62.76 (2.67)	46.87 (9.28)	68.62 (7.45)	69.35 (4.76)	71.82 (2.78)	63.32 (2.60)	67.91 (4.23)
Heat of reaction (kJ/mol)	42.10 (2.13)	47.56 (1.05)	46.62 (0.77)	49.14 (1.15)	48.34 (2.81)	52.43 (0.63)	46.92 (1.35)
Fractional monomer conversion	0.7398 (0.04)	0.8332 (0.02)	0.8141 (0.01)	0.8525 (0.02)	0.8333 (0.05)	0.8981 (0.01)	0.7988 (0.02)
Fractional residual monomer	0.2602 (0.04)	0.1668 (0.02)	0.1859 (0.01)	0.1475 (0.02)	0.1667 (0.05)	0.1019 (0.01)	0.2012 (0.02)
Glass-transition temperature (°C)	104.07 (0.87)	102.99 (1.20)	104.32 (1.14)	103.46 (0.19)	104.48 (0.21)	105.36 (0.82)	106.27 (1.94)

**Table C.2: Viscosity characteristics of TSBCs modified with EG-DMA**

Shear Rate (1/s)	Control (Pa·s)	2.5EGDMA (Pa·s)	5EGDMA (Pa·s)	10EGDMA (Pa·s)	15EGDMA (Pa·s)	20EGDMA (Pa·s)	25EGDMA (Pa·s)
0.4		1606 (203.2)	2366 (567.9)	2152 (274.9)	1716 (224.2)	2032 (99.67)	3689 (270.1)
0.6		1324 (160.1)	1792 (88.24)	1850 (120.5)	1588 (230.9)	1897 (166.3)	4101 (583.0)
0.8	1137 (60.88)	1253 (227.0)	1672 (90.00)	1776 (112.4)	1581 (178.0)	1822 (151.0)	3103 (335.1)
1.0	1029 (59.91)	1204 (291.4)	1617 (86.08)	1702 (103.1)	1440 (156.5)	1791 (151.9)	
1.2	903.5 (48.47)	1199 (319.6)	1536 (114.9)	1672 (129.6)	1426 (129.9)	1745 (125.1)	
1.6	751.8 (56.43)	1042 (226.7)	1364 (145.1)	1583 (162.1)	1351 (131.1)	1652 (94.90)	
2.0	636.8 (65.65)	927.1 (157.1)	1225 (173.5)	1463 (158.9)	1304 (120.9)	1582 (96.64)	
2.4	566.4 (93.38)	860.1 (132.6)	1126 (192)	1330 (152.1)	1198 (128.4)	1482 (54.46)	

## References

1. Kühn K-. Bone Cements: Up-to-Date Comparison of Physical and Chemical Properties of Commercial Materials. 1st ed. Germany: Springer-Verlag; 2000.
2. Breusch SJ, Kühn K-. Bone cements based on polymethylmethacrylate. *Orthopade*. 2003;32(1):41-50.
3. Hasenwinkel JM, Lautenschlager EP, Wixson RL, Gilbert JL. A novel high-viscosity, two-solution acrylic bone cement: Effect of chemical composition on properties. *J Biomed Mater Res*. 1999;47(1):36-45.
4. Eriksson RA, Albrektsson T. The effect of heat on bone regeneration: An experimental study in the rabbit using the bone growth chamber. *J Oral Maxillofac Surg*. 1984;42(11):705-11.
5. Vaishya R, Chauhan M, Vaish A. Bone cement. *J Clin Orthop Traum*. 2013;4(4):157-63.
6. Lewis G. Properties of acrylic bone cement: State of the art review. *J Biomed Mater Res*. 1997;38(2):155-82.
7. Seyfarth M, Werner K. Problems of residual monomer content in various bone cements. *Beitr Orthop Traumatol*. 1976;23(4):227-31.
8. Huiskes R. Mechanical failure in total hip arthroplasty with cement. *Curr Orthop*. 1993;7(4):239-47.
9. Wixson RL, Lautenschlager EP, Novak MA. Vacuum mixing of acrylic bone cement. *J Arthroplasty*. 1987;2(2):141-9.
10. Deb S, Vazquez B, Bonfield W. Effect of crosslinking agents on acrylic bone cements based on poly(methylmethacrylate). *J Biomed Mater Res*. 1997;37(4):465-73.
11. Deb S, Braden M, Bonfield W. Effect of crosslinking agents on poly(ethylmethacrylate) bone cements. *J Mater Sci Mater Med*. 1997;8(12):829-33.
12. Shim JB, Warner SJ, Hasenwinkel JM, Gilbert JL. Analysis of the shelf life of a two-solution bone cement. *Biomaterials*. 2005;26(19):4181-7.
13. Rodrigues DC, Ordway NR, Ru-Jyu Ma C, Fayyazi AH, Hasenwinkel JM. An ex vivo exothermal and mechanical evaluation of two-solution bone cements in vertebroplasty. *Spine J*. 2011;11(5):432-9.
14. Rodrigues DC. Development and characterization of multi-solution bone cements containing cross-linked pmma nanospheres and nanospherical polymer brushes [dissertation]. Syracuse University; 2010.

15. Min K, Silberstein M, Aluru NR. Crosslinking PMMA: Molecular dynamics investigation of the shear response. *J Polym Sci Part B*. 2014;52(6):444-9.
16. Alves NM, Gómez Ribelles JL, Mano JF. Enthalpy relaxation studies in polymethyl methacrylate networks with different crosslinking degrees. *Polymer*. 2005;46(2):491-504.
17. Sasaki T, Uchida T, Sakurai K. Effect of crosslink on the characteristic length of glass transition of network polymers. *J Polym Sci Part B*. 2006;44(14):1958-66.
18. Mathias LJ, Steadman S, Anderson K, Davis R, Jarrett W, Redfearn RD, et al. Gel-state NMR investigation of crosslinked poly(methyl methacrylate) incorporating  $^{13}\text{C}$  labeled ethylene glycol dimethacrylate. *Macromol Sympos*. 1999;141:47-55.
19. Yang J-, Lu C-, Hsu Y-, Shih C-. Mechanical properties of acrylic bone cement containing PMMA-SiO<sub>2</sub> hybrid sol-gel material. *J Biomed Mater Res*. 1997;38(2):143-54.
20. Vallo CI, Abraham GA, Cuadrado TR, San Román J. Influence of cross-linked PMMA beads on the mechanical behavior of self-curing acrylic cements. *J Biomed Mater Res Part B Appl Biomater*. 2004;70(2):407-16.
21. Vallo CI. Influence of filler content on static properties of glass-reinforced bone cement. *J Biomed Mater Res*. 2000;53(6):717-27.
22. Zuk A, Wejchan-Judek M, Balewski L. Devices to improving the techniques of preparing PIC. *Cem Concr Res*. 1984;14(4):559-64.
23. Gomoll AH, Fitz W, Scott RD, Thornhill TS, Bellare A. Nanoparticulate fillers improve the mechanical strength of bone cement. *Acta Orthop*. 2008;79(3):421-7. 24. Sperling LH. Introduction to Physical Polymer Science: Fourth Edition. In: Introduction to Physical Polymer Science: Fourth Edition. ; 2005. p. 1-845.
24. Sperling LH. Introduction to Physical Polymer Science: Fourth Edition. In: Introduction to Physical Polymer Science: Fourth Edition. ; 2005. p. 1-845.
25. ASTM F451-991. Standard Specification for Acrylic Bone Cement. 2007e1.
26. ASTM E399-83. Standard Test Method for Plane-strain fracture toughness of metallic materials. 1984.
27. ASTM D790-86. Standard Test Methods for Flexural Properties. 1986.
28. Vallo CI, Montemartini PE, Cuadrado TR. Effect of residual monomer content on some properties of a poly (methyl methacrylate)-based bone cement. *J Appl Polym Sci*. 1998;69(7):1367-83.

29. Jašo V, Stoiljkovic D, Radicevic R, Bera O. Kinetic modeling of bulk free-radical polymerization of methyl methacrylate. *Polym J*. 2013;45(6):631-6.
30. Vallo CI. Residual monomer content in bone cements based on poly(methyl methacrylate). *Polym Int*. 2000;49(8):831-8.
31. ISO 5833:2002. Implants for surgery -- Acrylic resin cements. 2002.
32. Deb S, Vazquez B. The effect of cross-linking agents on acrylic bone cements containing radiopacifiers. *Biomaterials*. 2001;22(15):2177-81.
33. Wang CT, Pilliar RM. Fracture toughness of acrylic bone cements. *J Mater Sci* 1989;24:3725-38.
34. Lednický F, Pelzbauer Z. Morphology of the fracture surface layer of poly(methyl methacrylate) and the fracture mechanism. *J Polym Sci Part C Polym Symp*. 1972;38:375-86.
35. Franco-Marquès E, Méndez JA, Gironès J, Pèlach MA. Thermal and dynamic mechanical characterization of acrylic bone cements modified with biodegradable polymers. *J Appl Polym Sci*. 2013;128(5):3455-64.
36. Ruhé PQ, Hedberg EL, Padron NT, Spauwen PHM, Jansen JA, Mikos AG. Biocompatibility and degradation of poly(DL-lactic-co-glycolic acid)/calcium phosphate cement composites. *J Biomed Mater Res Part A*. 2005;74(4):533-44.
37. Shi M, Kretlow JD, Nguyen A, Young S, Scott Baggett L, Wong ME, et al. Antibiotic-releasing porous polymethylmethacrylate constructs for osseous space maintenance and infection control. *Biomaterials*. 2010;31(14):4146-56.
38. Moore WR, Graves SE, Bain GI. Synthetic bone graft substitutes. *ANZ J Surg*. 2001;71(6):354-61.
39. Sony S, Suresh Babu S, Nishad KV, Varma H, Komath M. Development of an injectable bioactive bone filler cement with hydrogen orthophosphate incorporated calcium sulfate. *J Mater Sci Mater Med*. 2015;26(1):1-14.
40. Rudugier J, Kirsschner P, Richter IE, Schweikert, CH. Influence of different X-ray contrast materials and strength of bone cement. In: Hastings GW WD, editor. *Mechanical properties of biomaterials*. New York: Wiley; 1980.

**Vita**

NAME OF AUTHOR: Michael Wiegand

PLACE OF BIRTH: Rockford, Illinois

DATE OF BIRTH: June 6<sup>th</sup>, 1991

UNDERGRADUATE SCHOOL ATTENDED: Clarkson University

DEGREE AWARDED: Bachelor of Science in Chemical Engineering, May 2013

Minor in Biomedical and Rehabilitation Engineering

Minor in Chemistry

**AWARDS AND HONORS:**

Dean's List, Clarkson University, Fall 2009, Fall 2011-Spring 2013

Men's Varsity Golf Team Four Year Letter Winner, 2009-2013

**PROFESSIONAL EXPERIENCE:**

Research Assistant, 2013-2017, Department of Biomedical and Chemical Engineering, Syracuse University, Syracuse, NY

Engineering Technician Intern, 2012, Bristol-Myers Squibb: Upstream Manufacturing Sciences and Technology Department, Syracuse, NY